IEEE Journal of Translational Engineering in Health and Medicine

Received 15 December 2023; revised 7 March 2024, 4 April 2024, and 9 April 2024; accepted 10 April 2024.
Date of publication 15 April 2024; date of current version 24 April 2024.

Digital Object Identifier 10.1109/JTEHM.2024.3388561

Modeling Physical Forces Experienced by Cancer and Stromal Cells Within Different Organ-Specific Tumor Tissue

MORGAN CONNAUGHTON AND MAHSA DABAGH

Department of Biomedical Engineering, University of Wisconsin-Milwaukee, Milwaukee, WI 53211, USA

CORRESPONDING AUTHOR: M. DABAGH (dabaghme@uwm.edu)

This work was supported in part by the University of Wisconsin-Milwaukee under Project 101-193590-AAI3246-4 and in part by the Office of Undergraduate Research (OUR) for proving Support for Undergraduate Research Fellows (SURF).

ABSTRACT Mechanical force exerted on cancer cells by their microenvironment have been reported to drive cells toward invasive phenotypes by altering cells' motility, proliferation, and apoptosis. These mechanical forces include compressive, tensile, hydrostatic, and shear forces. The importance of forces is then hypothesized to be an alteration of cancer cells' and their microenvironment's biophysical properties as the indicator of a tumor's malignancy state. Our objective is to investigate and quantify the correlation between a tumor's malignancy state and forces experienced by the cancer cells and components of the microenvironment. In this study, we have developed a multicomponent, three-dimensional model of tumor tissue consisting of a cancer cell surrounded by fibroblasts and extracellular matrix (ECM). Our results on three different organs including breast, kidney, and pancreas show that: A) the stresses within tumor tissue are impacted by the organ specific ECM's biophysical properties, B) more invasive cancer cells experience higher stresses, C) in pancreas which has a softer ECM (Young modulus of 1.0 kPa) and stiffer cancer cells (Young modulus of 2.4 kPa and 1.7 kPa) than breast and kidney, cancer cells experienced significantly higher stresses, D) cancer cells in contact with ECM experienced higher stresses compared to cells surrounded by fibroblasts but the area of tumor stroma experiencing high stresses has a maximum length of 40 μm when the cancer cell is surrounded by fibroblasts and 12 μm for when the cancer cell is in vicinity of ECM. This study serves as an important first step in understanding of how the stresses experienced by cancer cells, fibroblasts, and ECM are associated with malignancy states of cancer cells in different organs. The quantification of forces exerted on cancer cells by different organ-specific ECM and at different stages of malignancy will help, first to develop theranostic strategies, second to predict accurately which tumors will become highly malignant, and third to establish accurate criteria controlling the progression of cancer cells malignancy. Furthermore, our *in silico* model of tumor tissue can yield critical, useful information for guiding *ex vivo* or *in vitro* experiments, narrowing down variables to be investigated, understanding what factors could be impacting cancer treatments or even biomarkers to be looking for.

INDEX TERMS Cancer cells, cell mechanics, forces on cells, ECM, fibroblasts, malignancy, tumor microenvironment.

I. INTRODUCTION

CANCER is one of the leading causes of death worldwide and in 2022 alone it accounted for about 10 million deaths [1]. The low cancer survival rate stems partly from the lack of capability, in both experimental and computational models, to predict whether a treatment will work for a specific patient. However, having knowledge on the malignancy state of a tumor may guide the physicians to decide on a treatment that will work [2], [3], [4], [5], [6], [7], [8], [9], [10], [11], [12]. A defining characteristic of this capability is a quantitative assessment of the malignancy state of a patient-specific tumor rather than qualitative evaluation. Thus, there have been intensive attempts to explore the indicators of tumors' malignancy which require models to replicate complexity and heterogeneity of a tumor tissue as observed in a human tumor, estimate alterations of individual components of tumor tissue,

determine mechanisms driving these alterations, and leverage this knowledge to link the components' alterations to the malignancy of the tumor. This study serves as an important first step in developing a quantitative assessment of a tumor's malignancy state.

Several models—-including *in* vitro [13], [14], [15], [16], [17], [18], in vivo [16], [17], [18], ex vivo [15], [19], mathematical, and in silico [20], [21], [22], [23], [24], [25], [26], [27], [28], [29], [30], [31], [32], [33], [34], [35], [36], [37], [38] —-have been developed to replicate human tumor tissue. Unfortunately, these models are limited because in vitro models still have the main challenge of fabricating an appropriate extracellular matrix (ECM) for specific tumors [13], [14], [15], [16], [17], [18]; in vivo models must recapitulate a human-like tumor progression and present a similar stroma as observed in human patients [16], [18]; ex vivo models with fixed tissues must be informative of the behavior of live tissue [15], [19]. In mathematical models, the main challenge is in translating results to human clinical treatment because they are not calibrated to a particular type of cancer [16], [18], [20], [21], [22], [23], [24], [25], [26], [27]. Mathematical models mostly apply the same criteria for tumor regression patterns across a wide range of tumor types, and differences between tumor sites and treatment modalities are not considered [24], [28], [29], [30], [31]. While mathematical models allow for safe and efficient control of features and parameters influencing tumor progression, their reproducibility and cost efficiency are limited by the initial tumor geometry and the calibration to a specific human tumor [32]. One additional note is that the selection of the modeling method is guided by the system's required observations (e.g., tissue behavior, drug particles' penetration, activation of adhesion proteins between tissue components) or measurements (e.g., components' remodeling, size, shape, forces experienced by components). While *in vitro* and *ex vivo* models enable the study of only a few factors of interest at any one time, *in silico* models enable a better understanding of the different factors individually as well as their interactions. *In silico* models of tissues have served as investigational platforms for a wide range of human diseases from wound healing to cancer [24], [30], [31], [33], [34], [35], [36], [37], [38]. Many of these platforms display unique and tunable capability such as mechanical properties of individual tissue components. In this study, we have developed a multicomponent, three-dimensional model of tumor tissue consisting of a cancer cell surrounded by fibroblasts and ECM.

Several studies have tried to identify biomarkers that are correlated with the malignancy degree of cancer cells [2], [3], [4], [5], [6], [7], [8], [9], [10], [11], [12]. Cancer cell migration, cancer cell volume, and compressive forces experienced by cancer cells are among the major biomarkers; for example, malignant cancer cells have shown increased expression of genes involved in cell motility compared to non-malignant cancer cells [2], [3], [4], [5], [6], [7], [8], [9], [10], [11], [12]. Cell migration requires many factors, such as the cytoskeleton, cell-matrix adhesion and cell volume regulation [6]. Cell volume regulation and the ion/water transport systems are main factors in cell migration because A) transport proteins, such as ion channels, ion carriers, and aquaporins, are indispensable for cell volume regulation under steady-state conditions and during exposure to osmotic stress, and B) several studies have revealed that cell volume regulation also plays an important role in the process of cell migration [7], [11], [12]. On the other hand, compressive stresses exerted on a cancer cell (mammary epithelial cell) by its microenvironment have been shown to drive cancer cells toward a malignant phenotype by altering cells' motility, cell proliferation, and cell apoptosis [5], [39], [40], [41], [42], [43], [44], [45], [46], [47], [48]. Over the past two decades, the role of mechanical phenotype of the cancer cells, their stroma, and ECM has been more appreciated [5], [39], [40], [41], [42], [43], [44], [45], [46], [47], [48]. These phenotypes are reflected in both cells and stroma's structure and mechanics and in the biophysical properties of the cells' microenvironment, such as the mechanics and topology of the ECM. The dynamic interactions between the biophysical properties of cells, stroma, and ECM establishes a dynamic, mechanical reciprocity between the cells and their surroundings in which the cells are able to exert contractile stresses against the extracellular environment. These forces, in turn, will regulate a wide range of cellular properties that are all critical to tumorigenesis, including size, shape, volume, motility, proliferation, and differentiation.

In this study, using our model of tumor tissue, we have first investigated how location of a cancer cell influences the stresses on fibroblasts and ECM, then quantified the impact of cancer cell stiffness on its microenvironment, and finally determined how these stresses may change in different organ-specific ECMs'. Our study examines and quantifies, for the first time, the impact of cancer cell location and its stiffness on local stresses within three different organs (breast, kidney, and pancreas. We have conducted simulations by developing an idealized geometry of tumor tissue consisting of a cancer cell, fibroblasts, and ECM to investigate the local stresses around a cancer cell within a tumor tissue. The model's input parameters, which depend on the tumor's malignancy, will be determined for each tumor tissue, based on ECM, fibroblasts, and the cancer cell's mechanical properties. This study assumes that the ECM is as a homogeneous media not including important microvascular structures seen within the ECM, such as fiber-forming elements (collagen and elastin) surrounded by various filling molecules (glycoproteins and proteoglycans), growth factors, and adhesion molecules. Moreover, the same properties were used for fibroblasts in all organ-specific tissues due to lack of available experimental data. To the best of our knowledge, no previous study investigated organ-specific stresses in a tumor tissue by isolating the impact of a cancer cell, stromal cells, and ECM. We have examined three different ECMs representing kidney, breast, and pancreatic tissues. For each organ, we studied two differ-

IEEE Journal of Translational Engineering in Health and Medicine

ent cancer cell lines with different invasiveness status: A) for kidney, ACHN (kidney-adenocarcinoma) and A-498 (kidney-carcinoma) where ACHN is more invasive [49], [50], B) for breast, MCF-7(breast adenocarcinoma) and T47D (breast-ductal carcinoma) where T47D is more invasive [8], [52], C) for pancreas, PDAC, PANC-1(pancreas-pancreatic ductal adenocarcinoma) and MIA PaCa-2 (pancreas-pancreatic ductal adenocarcinoma) where PANC-1 is more invasive [2], [3], [53], [54], [55]. The importance of forces, as the indicators of a tumor's malignancy state, is hypothesized to be an alteration of the components' biophysical properties and their surrounding microenvironment. The findings of the current study shed light on critical role of tumor malignancy on the physical stresses experienced by tumor tissue components and potential role of stresses as a biomarker to assess a tumor's malignancy state.

II. METHODS

Figure 1A shows a schematic representation of a human tumor and its components [1], [22], [24], [25], [56], [57], [58]. In the present study, the geometric model included a single cancer cell, fibroblasts and the ECM. The geometric model is depicted in Figures 1B-E, and Movie 1. Each cell (either a cancer cell or fibroblasts represented as fibroblasts) within the tumor is represented as a hexagonal shape [59], [60], [61], [62], [63], [64], [65], [66]. Each individual cell has a length of 8.1 μm (X-axis), a width of 7.54 μm (Y-axis), and a height of 8.0 μm (Z-axis) [62], [63], [64], [65], [66], [67], [68], [69]. The ECM has a length 100 μm, 100 μm width, and 100 μm depth [1], [22], [56], [57], [58], [59], [60], [61], [62]. The cancer cell was either placed on the outside region of the tumor structure to depict cell-ECM interactions as seen in Figures 1B-C or the cancer cell was placed within the tumor completely surrounded by fibroblasts to depict cell-cell interactions as shown in Figures 1D-E. Since organ-specific cancer sites have various mechanical properties depending on location and organ function, we examined three different organ-specific sites, breast, kidney, and pancreas. The test ranges and the reference values of al mechanical parameters applied in the model are summarized in Table 1 [67], [68], [69], [70], [71], [72], [73], [74], [75], [76], [77], [78], [79], [80], [81]. All parameters used in this study are based on values reported by previous studies which provided a range of parameters for the cancer cells, fibroblasts, and ECM of different tissue types. We attempted to use references which use atomic force microscopy (AFM) to measure the Young's modulus because the mechanical testing method may significantly affect the overall values for reported parameters. Here are few examples of our references and their mechanical testing method: one study used AFM to assess the Young's modulus of pancreas ECM [76], another study used AFM to measure the Young's modulus of kidney cell lines from different tumor types (carcinoma (A-498) and adenocarcinoma (ACHN)) [44], another study used AFM to measure the Young's modulus of breast ECM [73], and another study used AFM to measure the Young's modulus of fibroblasts [35], [36], [69]. In some cases, we used a specific value for a parameter which has been widely used previously, even though a range was given by few studies. In other cases, we used an average value for a parameter to best represent the impact of one parameter. ECM is modeled as a viscoelastic material using the Standard Linear Model [74], [75], [76], [77], [78], [79], [80] whereas fibroblasts and the organ-specific cancer cell lines are modeled as elastic material [34], [35], [68], [69], [70], [71], [72], [73], [74], [75]. We considered two distinct cancer cell lines for each of the organ-specific sites, as: 1) adenocarcinoma (MCF-7) [30], [37], [8], [52], 2) invasive ductal carcinoma (T47D) [8], [30], [37], [38], [52], 3) carcinoma (A-498) [24], [30], [49], [50], [51], 4) adenocarcinoma (ACHN) [24], [30], [49], [50], [51], 5) PANC-1 [2], [3], [30], [52], [53], [54], [55], 6) MIA PaCa-2 [2], [3], [30], [52], [53], [54], [55]. Note that A498 has been reported to be non-metastasis whereas ACHN are known as metastatic RCC cells, T47D is reported to be slightly more invasive than MCF7, and PANC-1 is reported to be more invasive than MIA-PaCa2. As seen in Table 1,the breast cancer cell line T47D has a Young's modulus of 1.2 kPa whereas MCF-7 has a Young's modulus of 0.4 kPa, the kidney cancer cell line ACHN has a Young's modulus of 7.41 kPa whereas A-498 has a Young's modulus of 2.48 kPa, and the pancreatic cancer cell line PANC-1 has a Young's modulus of 2.41 kPa whereas MIA-PaCa-2 has a Young's modulus of 1.7 kPa.

A MATLAB code (MATLAB v. R2021b) is applied to generate the geometry of the sinusoidal surface o cells. Model geometries are exported to the finite-element method solver via COMSOL MULTIPHYSICS v. 5.6 (COMSOL AB, Stockholm, Sweden). The models are solved using a stationary solver where simulations were performed on a Dell PRECISION, 16 processor computer, with 128 GB RAM. Post-processed results for stresses experienced by tumor tissue components are obtained and exported to MATLAB_R2021b for postprocessing.

All cellular components were assigne with material properties and mesh specifications. The computational results for the von Mises stress was determined and examined for independence of mesh density. Mesh independency was achieved by using a finer computational mesh consisting of 464,690 tetrahedral elements, 26,808 edge elements and 108,228 boundary elements for cells (including both fibroblasts and cancer cell) whereas ECM had 991,925 tetrahedral elements, 27,024 edge elements, and 112,920 boundary elements. At the upper side of ECM, a boundary load was added to the model to represent the blood pressure in capillaries as 10 mmHg or 20 mmHg (1,333 Pa and 2,666 Pa, respectfully) [82] whereas the lower boundary is set as fixed constraint.

All stress components are computed and applied to calculate the von Mises stresses (σ_{VMS}) a stress invariant usually referred as [59], [60], [61]

$$\sigma_{\mathrm{VMS}} = \{\frac{1}{2}[(\sigma_{\mathrm{xx}} - \sigma_{\mathrm{yy}})^2 + (\sigma_{\mathrm{xx}} - \sigma_{\mathrm{zz}})^2 + (\sigma_{\mathrm{yy}}$$

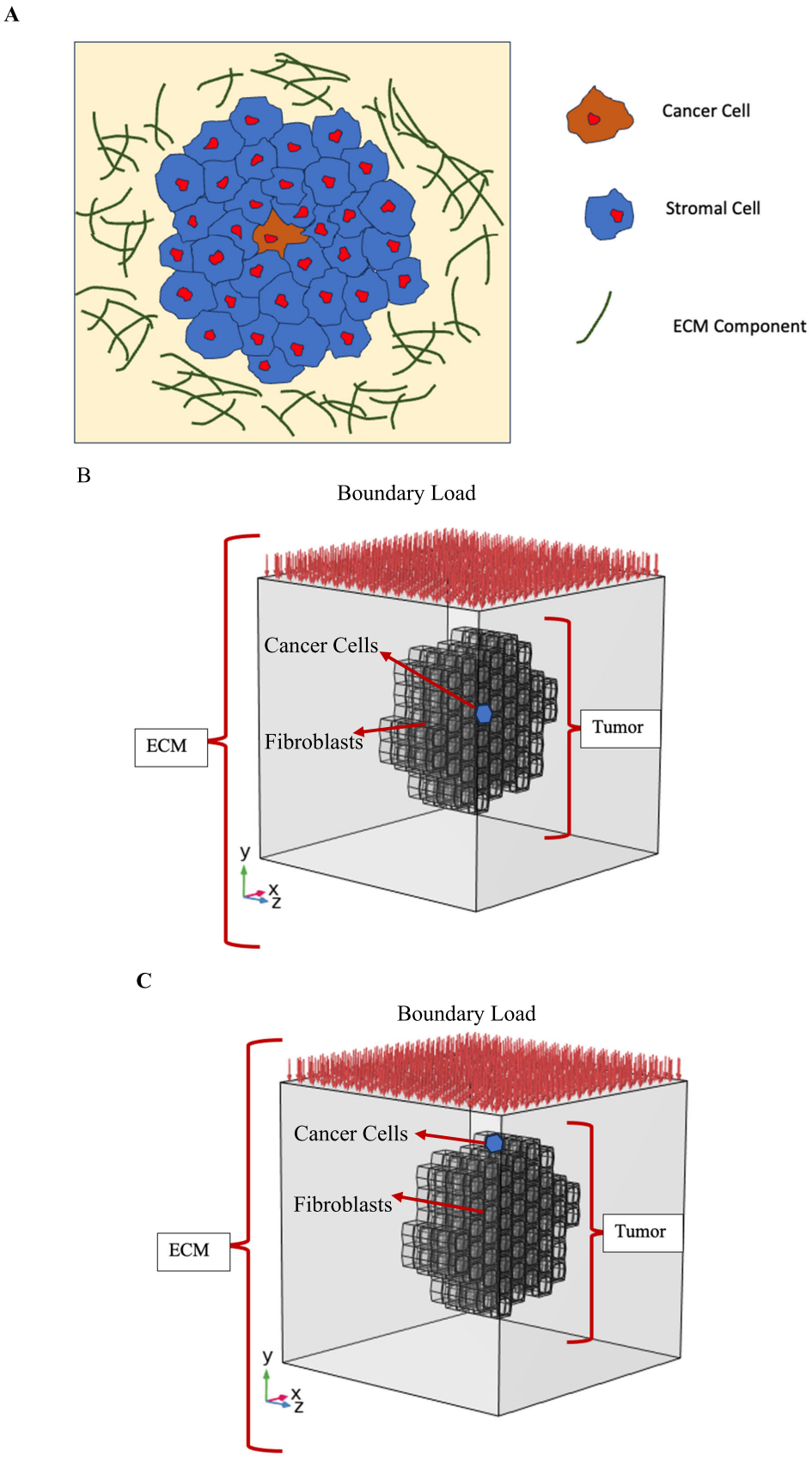

FIGURE 1. A) Schematic representation of a tumor tissue and its components. B) Three-dimensional model of the tumor microenvironment when a cancer cell is in contact the surrounding fibroblasts, C) when a cancer cell is in contact with the ECM.

IEEE Journal of Translational Engineering in Health and Medicine

TABLE 1. **Model parameters.**

Parameter	Literature range	Our setting	Ref.
E_{fibro}, kPa (Young's modulus of fibroblasts)	2.5-5	2.5	[35-36, 74]
E_{MCF7}, kPa (Young's modulus of MCF-7(Breast adenocarcinoma))	0.1-9.24	0.4	[30, 38, 53-54]
E_{T47D}, kPa (T47D (more invasive) (Breast-ductal carcinoma))	1.2-8.39	1.2	[30, 38-39, 53-54]
E_{ACHN}, kPa (ACHN (more invasive) (Kidney-adenocarcinoma))	1-7.41	7.41	[30-31, 50-52]
E_{A498}, kPa (A-498 (Kidney- carcinoma))	1-100	2.48	[30-31, 50-52
E_{PANC1}, kPa (PANC-1(Pancreas- pancreatic ductal adenocarcinoma), (more invasive))	0.5-2.4	2.4	[30, 54-59]
E_{PaCa2}, kPa (MIA PaCa-2 (Pancreas-pancreatic ductal adenocarcinoma))	0.5-1.7	1.7	[30, 54-59]
E_{Breast}, kPa (Breast ECM)	1.9-33	3.25	[43, 46]
E_{Kidney}, kPa (Kidney ECM)	5-20	7.5	[43, 48]
$E_{Pancreas}$, kPa (Pancreas ECM)	1.0	1.0	[45]
G_{Breast}, kPa (Shear modulus of Breast ECM)	0.5-25	1.09	[82-83]
G_{Kidney}, kPa (Kidney ECM)	N/A	2.51	[83]
$G_{Pancreas}$, kPa (Pancreas ECM)	N/A	0.33	[83]
K_{Breast}, kPa (Bulk modulus of Breast ECM)	N/A	108.3	[83]
K_{Kidney}, kPa (Kidney ECM)	N/A	250.0	[83]

TABLE 1. ***(Continued.)*** **Model parameters.**

$K_{Pancreas}$, kPa (Pancreas ECM)	N/A	33.3	[83]
T_{Breast}, ms (Relaxation Time of Breast ECM)	1680	1680	[84]
T_{Kidney}, ms (Kidney ECM)	1142-1314	1314	[85]
$T_{Pancreas}$, ms (Pancreas ECM)	725	725	[85]

$$- \sigma_{zz})^2 + 6(\sigma_{xy}^2 + \sigma_{xz}^2 + \sigma_{yz}^2)]\} \quad (1)$$

III. RESULTS

Figure 2 demonstrates the von Mises stress distribution for breast cancer cell lines, MCF-7 and T47D, the kidney cancer cell lines, ACHN and A-498, and the pancreatic cancer cell lines, PANC-1 and MIA PaCa-2. The boundary load applied to these studied cases is 10 mmHg (1,333Pa). Figure 2A, 2B, 2C show the stresses along the tissue width (x-axis) where the analysis domain is limited to the cancer cell's length (y-axis) and thickness (z-axis). Here, the cancer cell is in vicinity of ECM; Figure 2D shows the stresses along the tissue length (y-axis) when the cancer cell is in vicinity of ECM. Here, the analysis domain is limited to the cancer cell's width (x-axis) and thickness (z-axis); Figure 2E shows the stresses along the tissue thickness (z-axis) when the cancer cell is in vicinity of ECM. Here, the analysis domain is limited to the cancer cell's width (x-axis) and length (y-axis); Figure 2F, 2G, 2H show the stresses along the tissue width (x-axis) when the cancer cell is surrounded by fibroblasts; Figure 2I shows the stresses along the tissue length (y-axis) when the cancer cell is surrounded by fibroblasts; and Figure 2J demonstrates the stresses along the tissue thickness (z-axis) when the cancer cell is surrounded by fibroblasts.

Figures 3A-F show the von Mises stress distribution for MCF-7, T47D, ACHN, A-498, PANC-1, and MIA-PaCa-2 with an applied boundary load of 20 mmHg. Results are demonstrated for same panels shown in Figure 2-J.

A comparison between Figure 2B,2G and Figure 3B, and 3G shows that the pancreatic tissue with PANC-1 experienced stresses up to about 3,750 N/m^2 at 10 mmHg and once the pressure was doubled to 20 mmHg, the stress magnitude increased to about 7,500 N/m^2. This is also seen for tissues with MCF-7, T47D, ACHN, A-984, and MIA-PaCa-2, which increased from 1,400 to 2,800 N/m^2, 1,250 to 2,500 N/m^2, 600 N/m^2 to 1,200 N/m^2, 800 N/m^{2}to 1,600 N/m^2, and 3,800 to 7,700 N/m^2. This was also seen for the y-axis and z-axis depicted in Figures 2D, 2E, 2I, 2J, 3D, 3E, 3I, and 3J.

Figure 4 demonstrates the von Mises stress distribution across the tumor tissue, when the boundary load is set to 10 mmHg and the cancer cell is in vicinity of ECM. Note that Figures 4A-F show the stress distribution on one surface which passes through the cancer cell center at z-axis. Figures 4A-F demonstrate the von Mises stress distribution for: MCF-7 with a stiffness of 0.4 kPa, where the stiffness of the ECM is 3.25 kPa, B) T47D with a stiffness of 1.2 kPa where the ECM's stiffness is 3.25 kPa, C) ACHN with a stiffness of 7.41 kPa where the ECM's stiffness is 7.5 kPa, D) A-498 ECM with a stiffness 2.48 kPa where the ECM's stiffness is 7.5 kPa, E) PANC-1 with a stiffness of 2.4 kPa where the ECM's stiffness is 1.0 kPa, F) MIA-PaCa-2 with a stiffness 1.7 kPa where the stiffness of the ECM is 1.0 kPa.

Figure 5 demonstrates the von Mises stress magnitude averaged over whole tumor tissue. The x-axis is the ratio of ECM stiffness to cancer cell stiffness which is calculated based on the stiffness of for each organ and the stiffness of corresponding cancer cell type.

A. DISCUSSION

In this study, *in silico* models of pancreas, breast, and kidney tumor tissues were developed to investigate the physical forces exerted on a cancer cell by the ECM and fibroblasts, and how these forces are influenced by malignancy of the cancer cell. *In silico* models of tissues can serve as investigational platforms displaying unique and tunable capabilities such as the mechanical properties of tissue components [63], [83], [84], [85]. *In silico* models are the most commonly used computational approaches in clinical practice in which using patient-derived tumor model parameters could enhance the sensitivity and accuracy of the models [33], [36]. However, for personalized models, a deeper understanding of tumor physiology and dynamics is required. This demands the incorporation of a tumor tissue's cellular heterogeneity into the *in silico* models.

Several studies have tried to identify biomarkers that are correlated with the malignancy degree of cancer cells [2], [3], [4], [5], [6], [7], [8], [9], [10], [11], [12]. Cell migration, cell volume, and compressive forces experienced by cancer cells are among the major biomarkers; for example, malignant cancer cells have shown increased expression of genes involved in cell motility compared to non-malignant cancer cells [2], [3], [4], [5], [6], [7], [8], [9], [10], [11], [12]. Cell migration requires many factors, such as the cytoskeleton, cell-matrix adhesion and cell volume regulation [6]. Cell

IEEE Journal of Translational Engineering in Health and Medicine

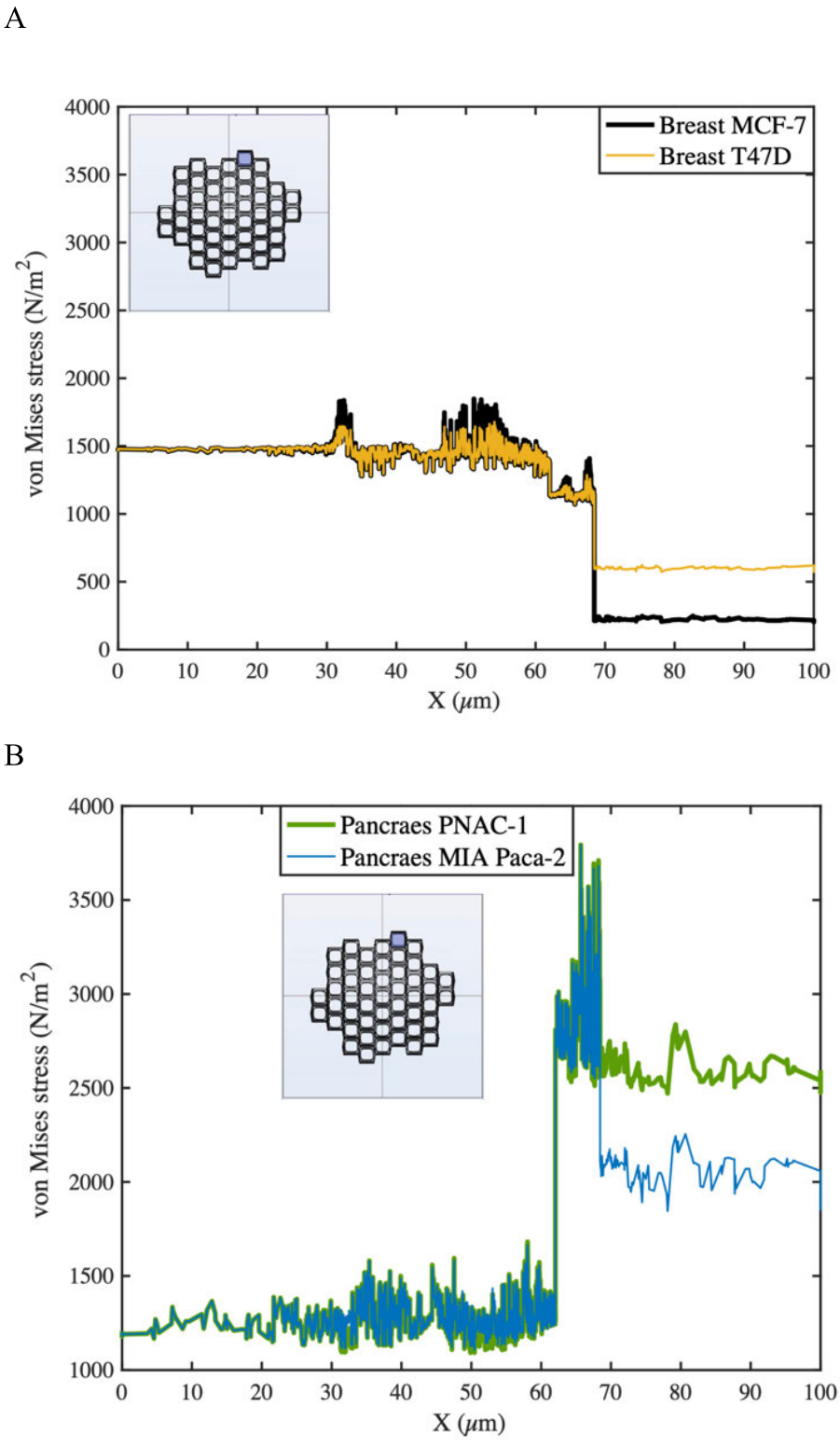

FIGURE 2. The von Mises stress distribution within tumor tissue when the cancer cells is surrounded by fibroblasts and when the cancer cell is in vicinity of ECM. Results are shown for breast cancer cell lines, MCF-7 and T47D, the kidney cancer cell lines, ACHN and A-498, and the pancreatic cancer cell lines, PANC-1 and MIA PaCa-2. Figures 2A,2B, 2C, 2F, 2G, and 2H show the stresses along the tissue width (x-axis); Figures 2D and 2I demonstrate the stresses along the tissue length (y-axis); Figures 2E and 2J show the stresses along the tissue thickness (z-axis). Note that a boundary load of 10 mmHg (1,333 Pa) is applied.

C

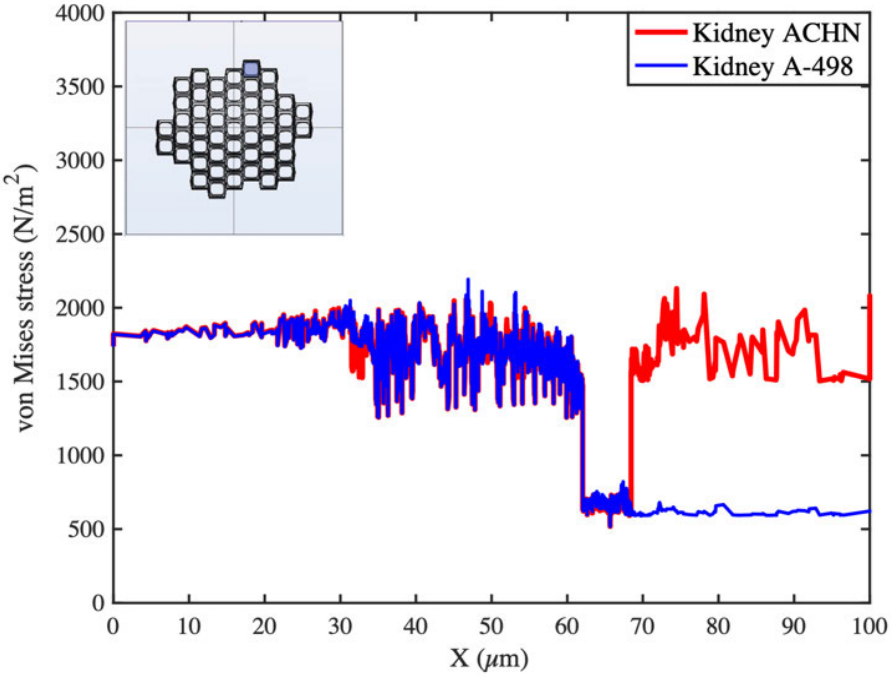

D

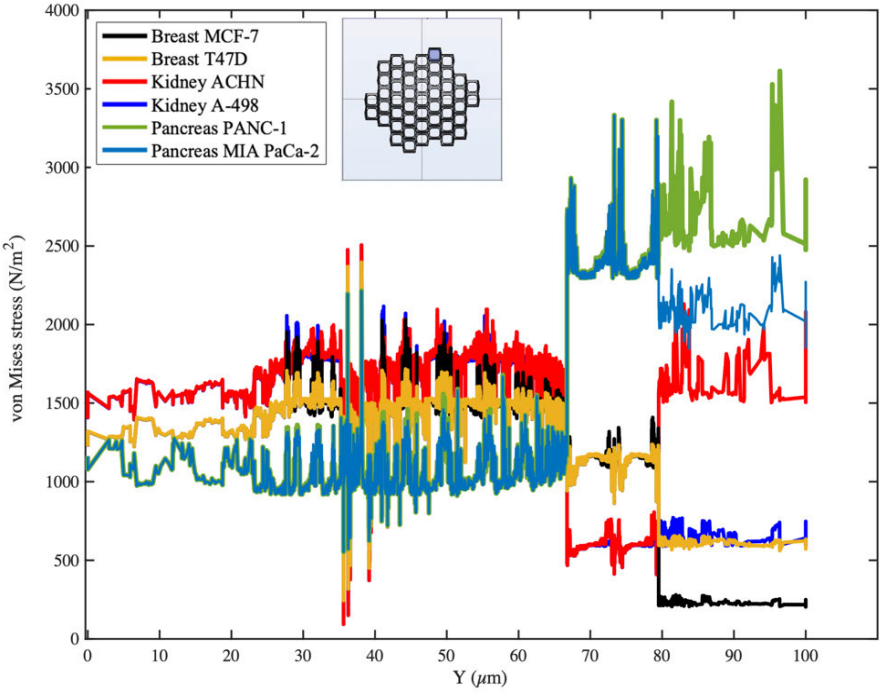

FIGURE 2. ***(Continued.)*** **The von Mises stress distribution within tumor tissue when the cancer cells is surrounded by fibroblasts and when the cancer cell is in vicinity of ECM. Results are shown for breast cancer cell lines, MCF-7 and T47D, the kidney cancer cell lines, ACHN and A-498, and the pancreatic cancer cell lines, PANC-1 and MIA PaCa-2. Figures 2A,2B, 2C, 2F, 2G, and 2H show the stresses along the tissue width (x-axis); Figures 2D and 2I demonstrate the stresses along the tissue length (y-axis); Figures 2E and 2J show the stresses along the tissue thickness (z-axis). Note that a boundary load of 10 mmHg (1,333 Pa) is applied.**

IEEE Journal of Translational Engineering in Health and Medicine

E

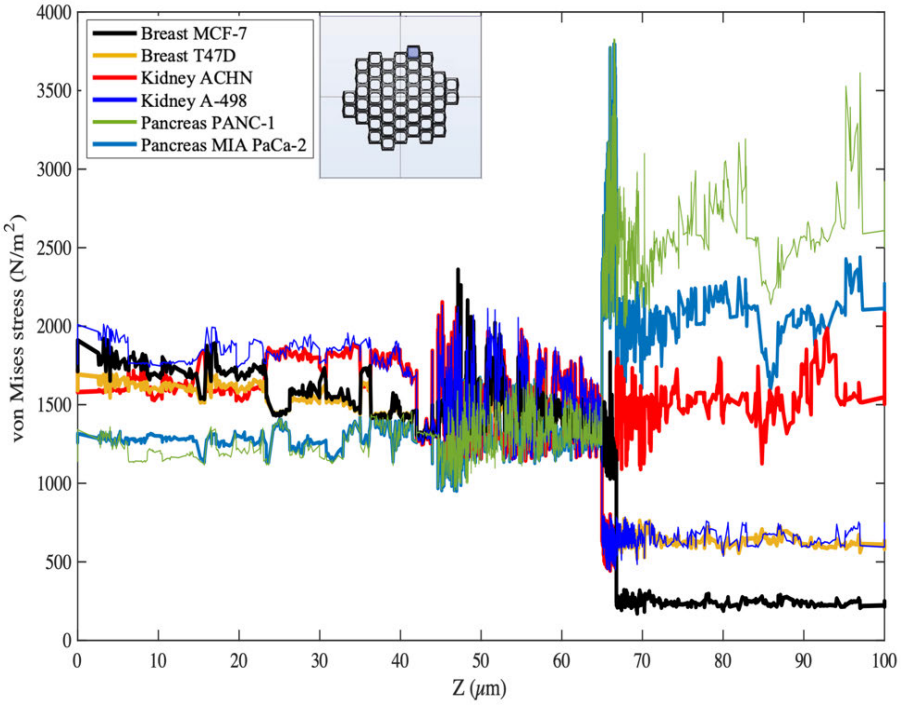

F

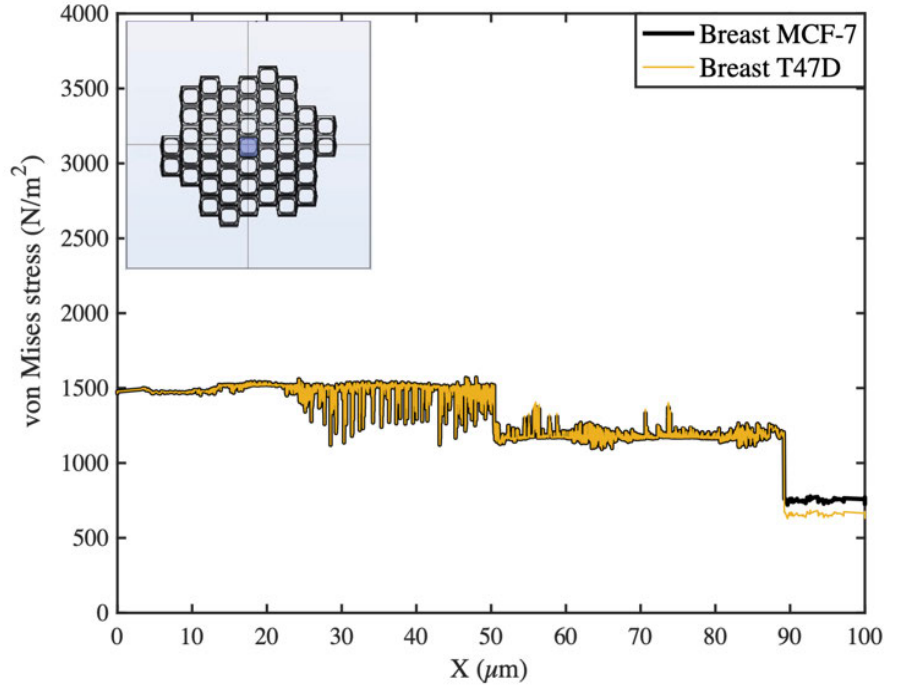

FIGURE 2. ***(Continued.)*** **The von Mises stress distribution within tumor tissue when the cancer cells is surrounded by fibroblasts and when the cancer cell is in vicinity of ECM. Results are shown for breast cancer cell lines, MCF-7 and T47D, the kidney cancer cell lines, ACHN and A-498, and the pancreatic cancer cell lines, PANC-1 and MIA PaCa-2. Figures 2A,2B, 2C, 2F, 2G, and 2H show the stresses along the tissue width (x-axis); Figures 2D and 2I demonstrate the stresses along the tissue length (y-axis); Figures 2E and 2J show the stresses along the tissue thickness (z-axis). Note that a boundary load of 10 mmHg (1,333 Pa) is applied.**

G

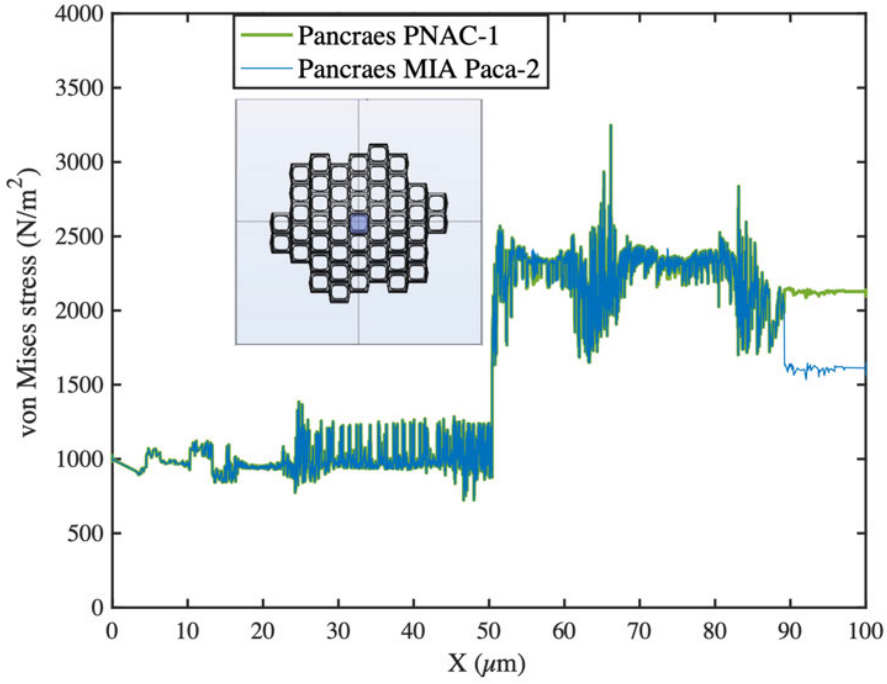

H

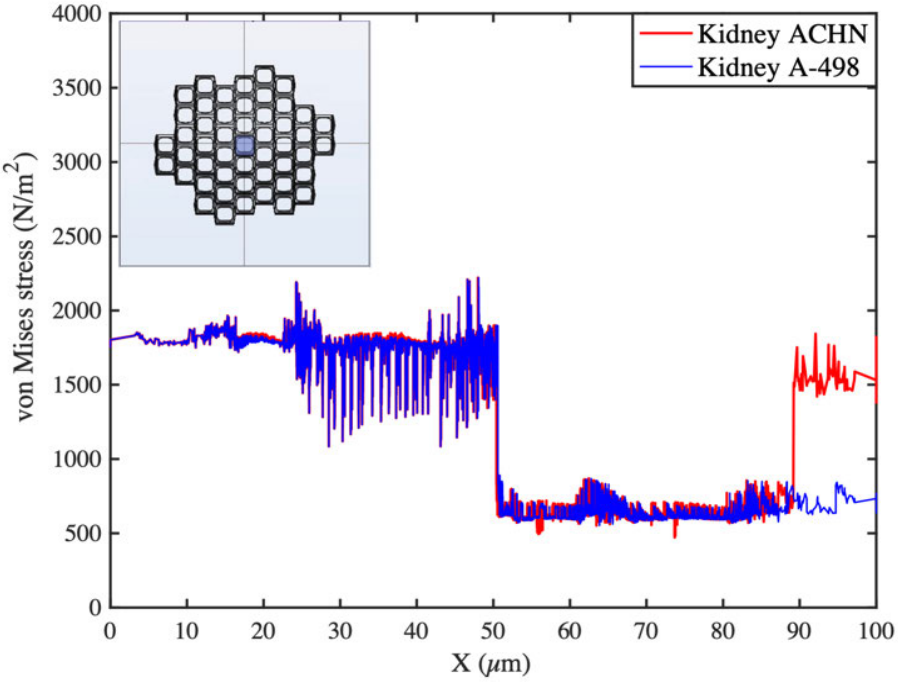

FIGURE 2. ***(Continued.)*** **The von Mises stress distribution within tumor tissue when the cancer cells is surrounded by fibroblasts and when the cancer cell is in vicinity of ECM. Results are shown for breast cancer cell lines, MCF-7 and T47D, the kidney cancer cell lines, ACHN and A-498, and the pancreatic cancer cell lines, PANC-1 and MIA PaCa-2. Figures 2A,2B, 2C, 2F, 2G, and 2H show the stresses along the tissue width (x-axis); Figures 2D and 2I demonstrate the stresses along the tissue length (y-axis); Figures 2E and 2J show the stresses along the tissue thickness (z-axis). Note that a boundary load of 10 mmHg (1,333 Pa) is applied.**

IEEE Journal of Translational Engineering in Health and Medicine

I

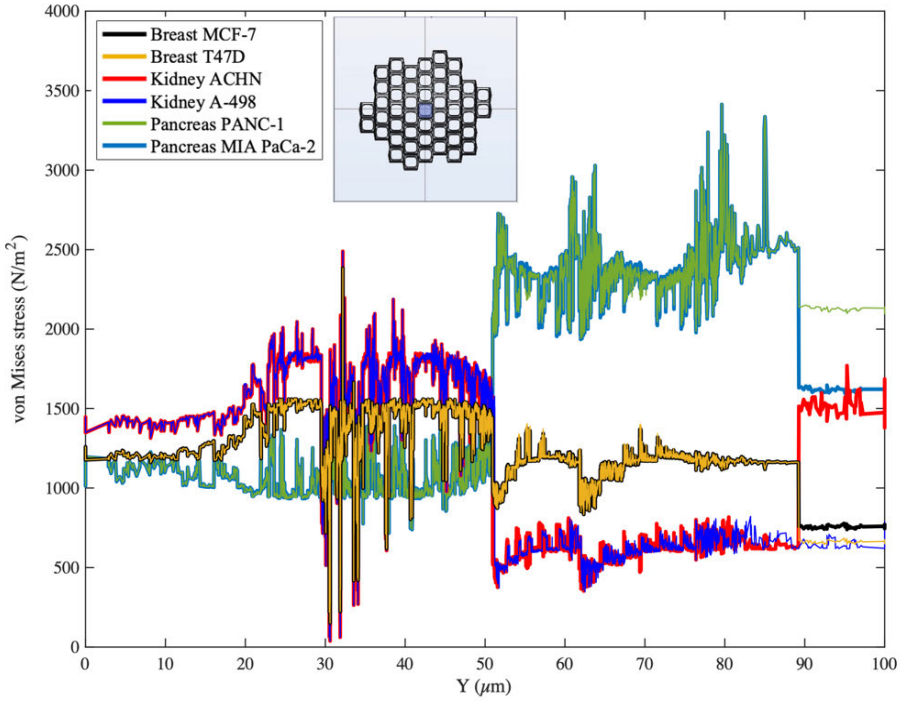

J

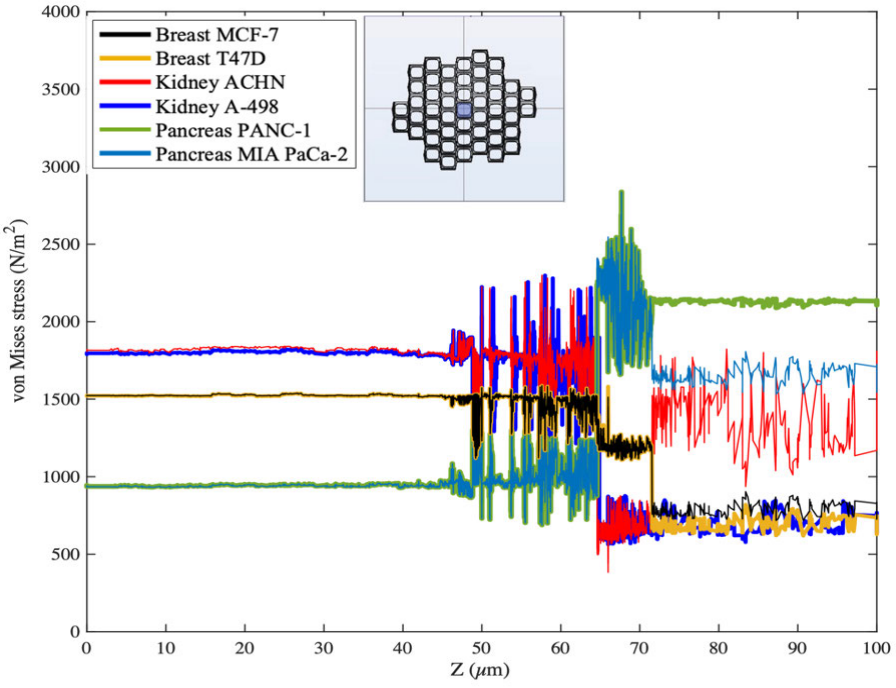

FIGURE 2. ***(Continued.)*** **The von Mises stress distribution within tumor tissue when the cancer cells is surrounded by fibroblasts and when the cancer cell is in vicinity of ECM. Results are shown for breast cancer cell lines, MCF-7 and T47D, the kidney cancer cell lines, ACHN and A-498, and the pancreatic cancer cell lines, PANC-1 and MIA PaCa-2. Figures 2A,2B, 2C, 2F, 2G, and 2H show the stresses along the tissue width (x-axis); Figures 2D and 2I demonstrate the stresses along the tissue length (y-axis); Figures 2E and 2J show the stresses along the tissue thickness (z-axis). Note that a boundary load of 10 mmHg (1,333 Pa) is applied.**

A

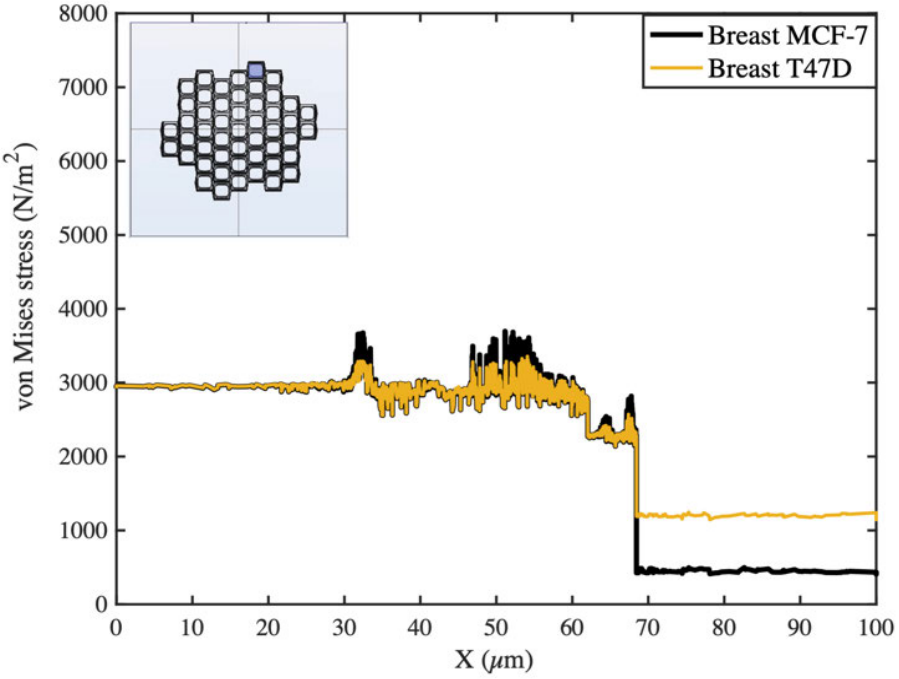

B

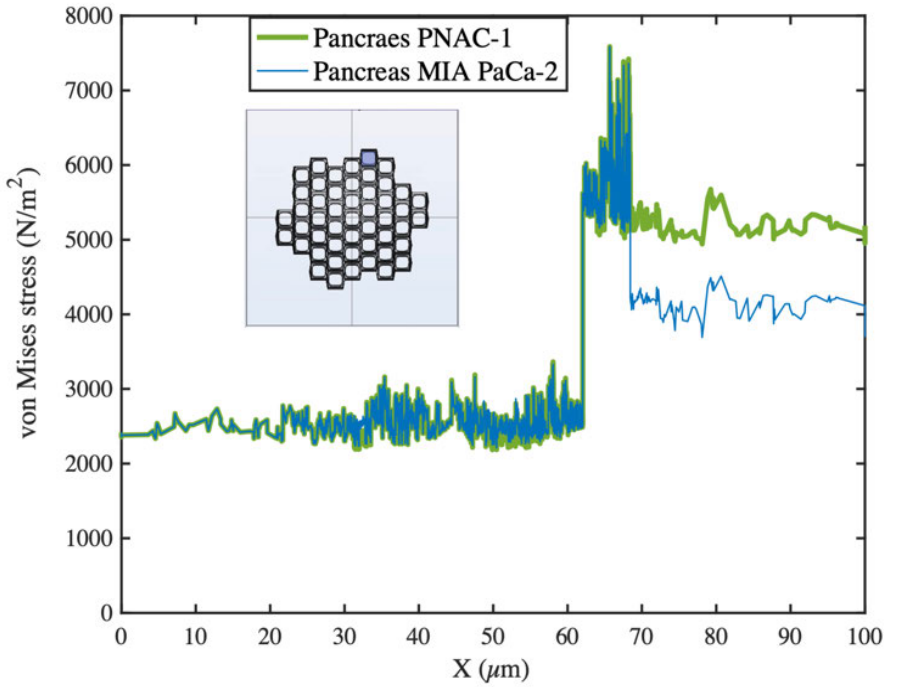

FIGURE 3. The von Mises stress distribution within tumor tissue when the cancer cells is surrounded by fibroblasts and when the cancer cell is in vicinity of ECM. Results are shown for breast cancer cell lines, MCF-7 and T47D, the kidney cancer cell lines, ACHN and A-498, and the pancreatic cancer cell lines, PANC-1 and MIA PaCa-2. Figures 3A, 3B, 3C, 3F, 3H, and 3G show the stresses along the tissue width (x-axis); Figures 3D and 3I demonstrate the stresses along the tissue length (y-axis); Figures 3E and 3J show the stresses along the tissue thickness (z-axis). Note that a boundary load of 20 mmHg (2,666 Pa) is applied.

IEEE Journal of Translational Engineering in Health and Medicine

C

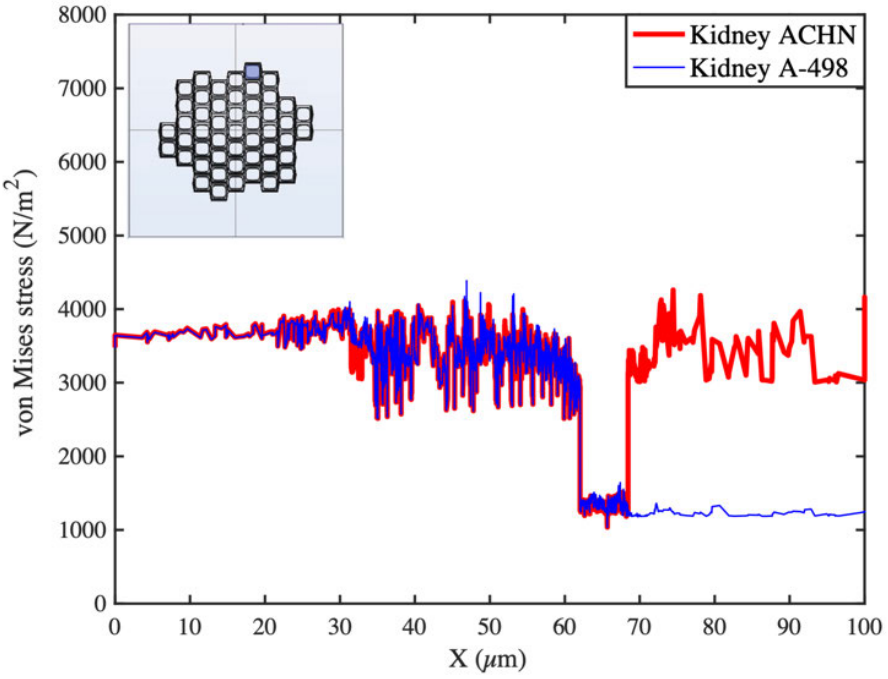

D

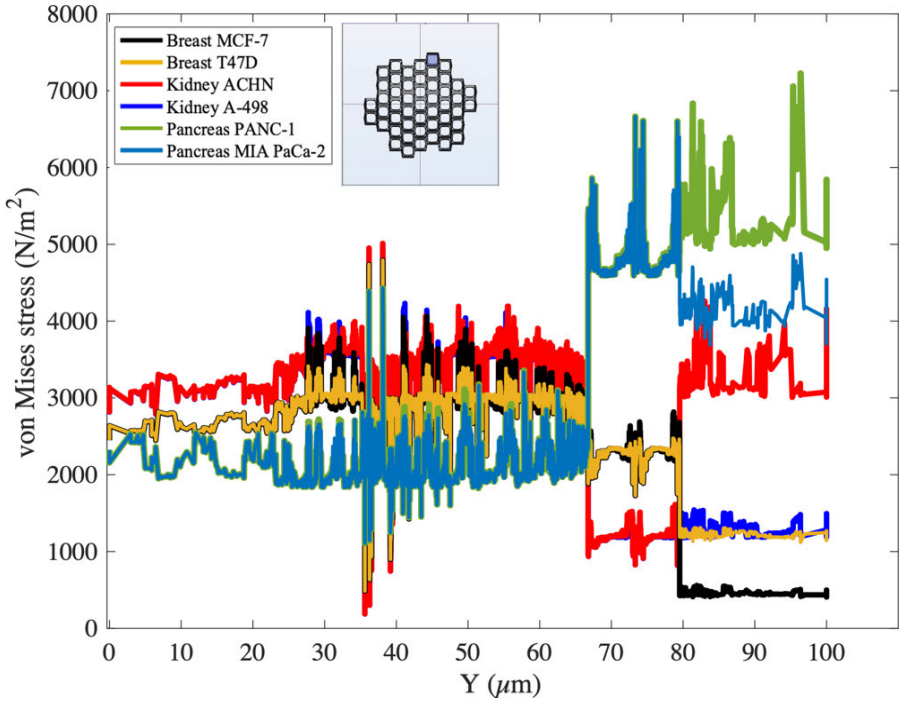

FIGURE 3. ***(Continued.)*** **The von Mises stress distribution within tumor tissue when the cancer cells is surrounded by fibroblasts and when the cancer cell is in vicinity of ECM. Results are shown for breast cancer cell lines, MCF-7 and T47D, the kidney cancer cell lines, ACHN and A-498, and the pancreatic cancer cell lines, PANC-1 and MIA PaCa-2. Figures 3A, 3B, 3C, 3F, 3H, and 3G show the stresses along the tissue width (x-axis); Figures 3D and 3I demonstrate the stresses along the tissue length (y-axis); Figures 3E and 3J show the stresses along the tissue thickness (z-axis). Note that a boundary load of 20 mmHg (2,666 Pa) is applied.**

E

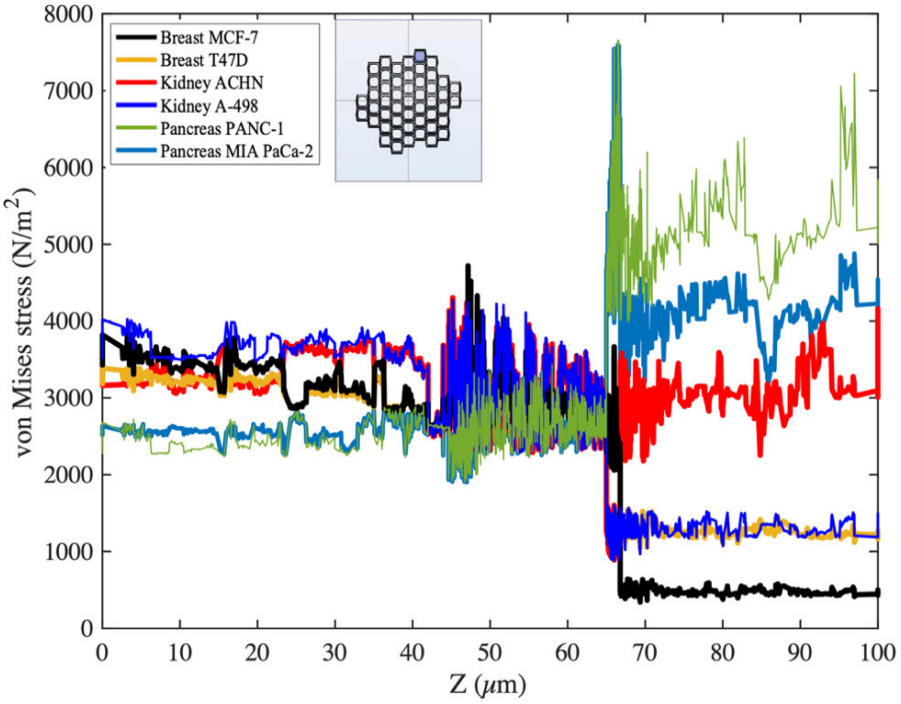

F

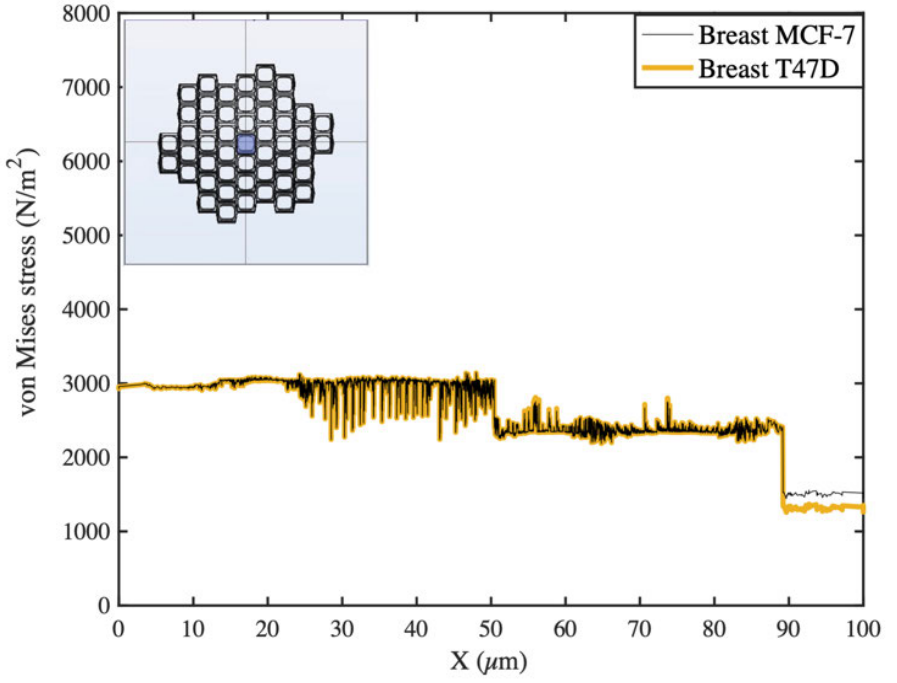

FIGURE 3. ***(Continued.)*** **The von Mises stress distribution within tumor tissue when the cancer cells is surrounded by fibroblasts and when the cancer cell is in vicinity of ECM. Results are shown for breast cancer cell lines, MCF-7 and T47D, the kidney cancer cell lines, ACHN and A-498, and the pancreatic cancer cell lines, PANC-1 and MIA PaCa-2. Figures 3A, 3B, 3C, 3F, 3H, and 3G show the stresses along the tissue width (x-axis); Figures 3D and 3I demonstrate the stresses along the tissue length (y-axis); Figures 3E and 3J show the stresses along the tissue thickness (z-axis). Note that a boundary load of 20 mmHg (2,666 Pa) is applied.**

IEEE Journal of Translational Engineering in Health and Medicine

G

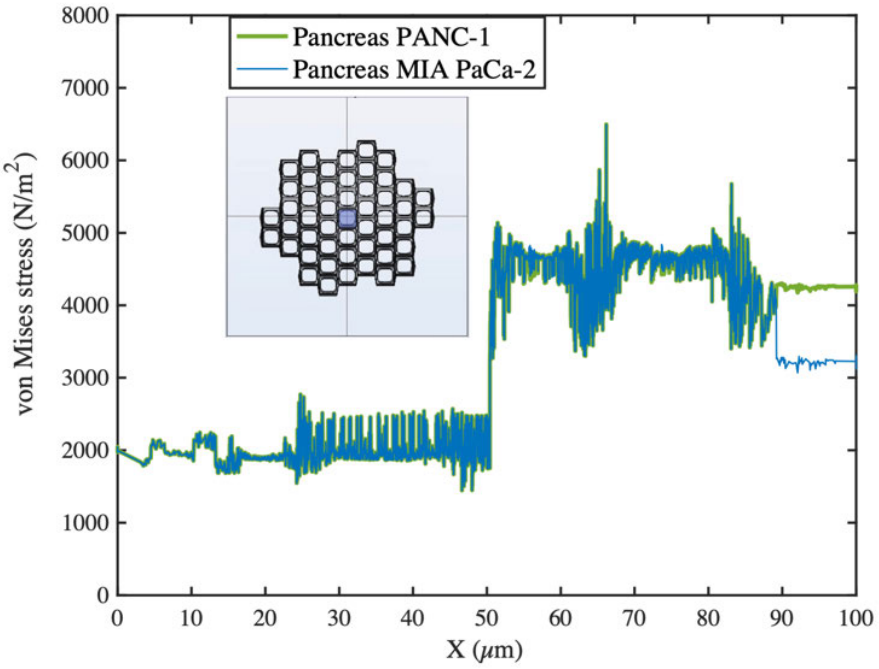

H

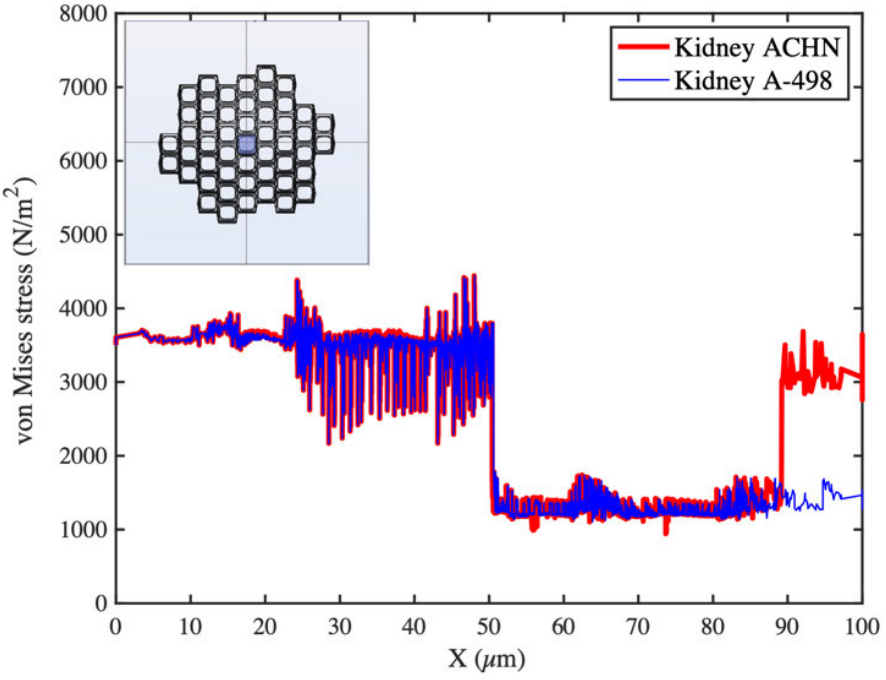

FIGURE 3. ***(Continued.)*** **The von Mises stress distribution within tumor tissue when the cancer cells is surrounded by fibroblasts and when the cancer cell is in vicinity of ECM. Results are shown for breast cancer cell lines, MCF-7 and T47D, the kidney cancer cell lines, ACHN and A-498, and the pancreatic cancer cell lines, PANC-1 and MIA PaCa-2. Figures 3A, 3B, 3C, 3F, 3H, and 3G show the stresses along the tissue width (x-axis); Figures 3D and 3I demonstrate the stresses along the tissue length (y-axis); Figures 3E and 3J show the stresses along the tissue thickness (z-axis). Note that a boundary load of 20 mmHg (2,666 Pa) is applied.**

I

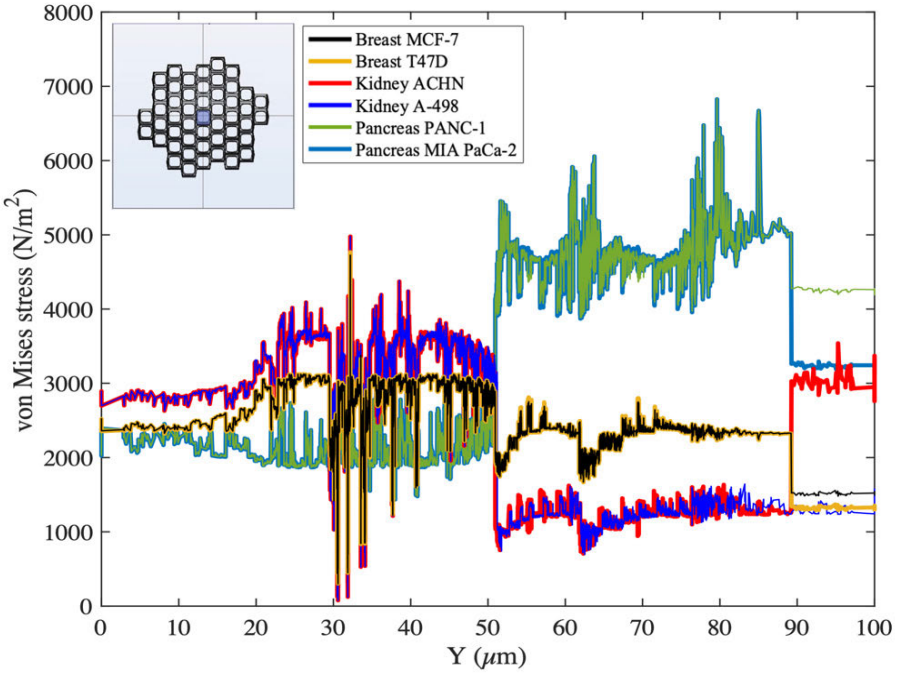

J

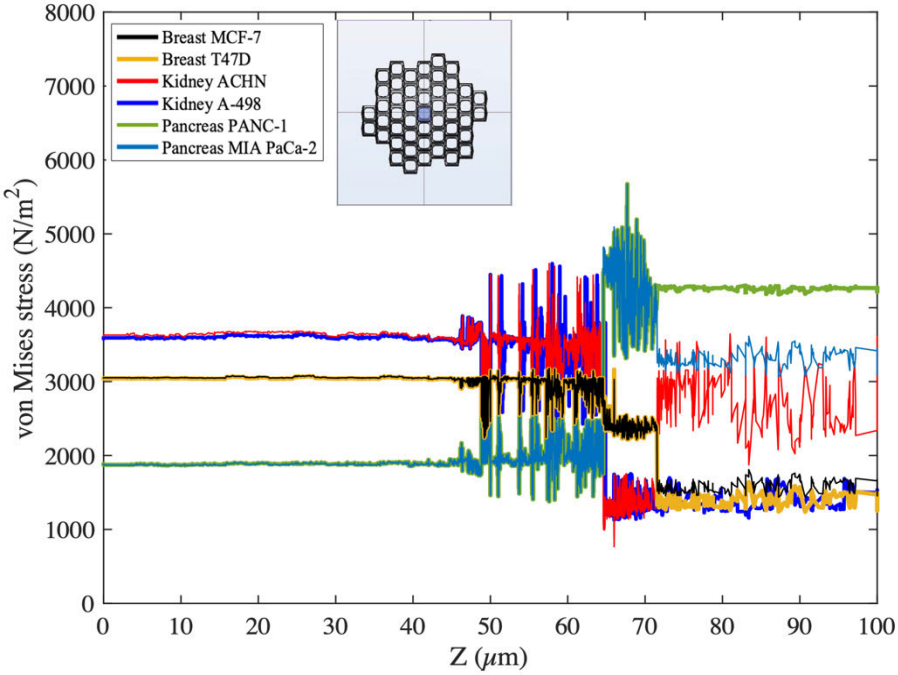

FIGURE 3. ***(Continued.)*** **The von Mises stress distribution within tumor tissue when the cancer cells is surrounded by fibroblasts and when the cancer cell is in vicinity of ECM. Results are shown for breast cancer cell lines, MCF-7 and T47D, the kidney cancer cell lines, ACHN and A-498, and the pancreatic cancer cell lines, PANC-1 and MIA PaCa-2. Figures 3A, 3B, 3C, 3F, 3H, and 3G show the stresses along the tissue width (x-axis); Figures 3D and 3I demonstrate the stresses along the tissue length (y-axis); Figures 3E and 3J show the stresses along the tissue thickness (z-axis). Note that a boundary load of 20 mmHg (2,666 Pa) is applied.**

IEEE Journal of Translational Engineering in Health and Medicine

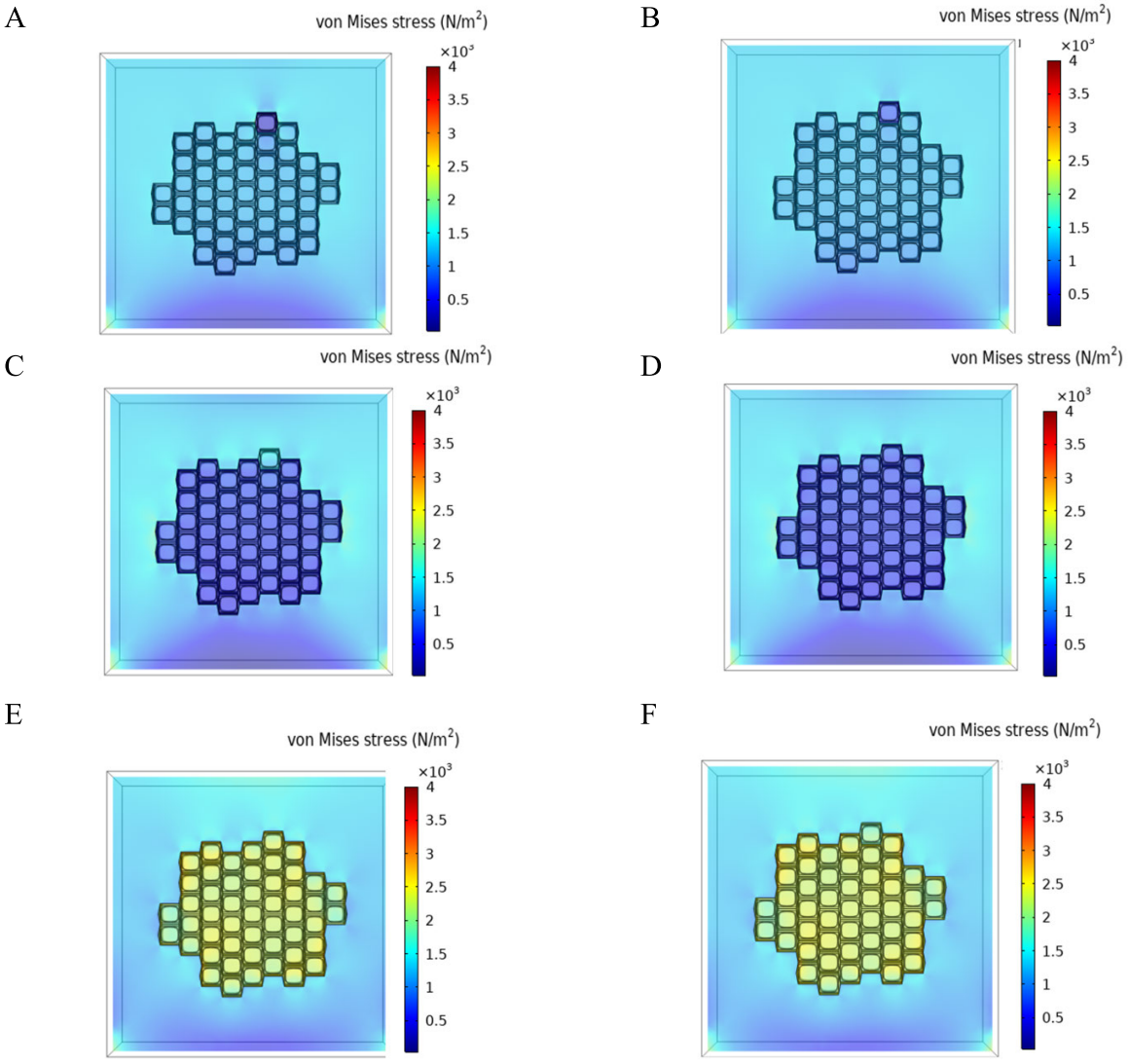

FIGURE 4. **The von Mises stress distribution across the tumor stroma with boundary load of 10 mmHg for A) breast tissue with MCF-7, B) breast tissue and T47D, C) kidney tissue with ACHN, D) kidney tissue with A-498 ECM, E) pancreas tissue with PANC-1, F) pancreas tissue with MIA-PaCa-2.**

volume regulation and the ion/water transport systems are main factors in cell migration because A) transport proteins, such as ion channels, ion carriers, and aquaporins, are indispensable for cell volume regulation under steady-state conditions and during exposure to osmotic stress, and B) several studies have revealed that cell volume regulation also plays an important role in the process of cell migration [7], [11]. Another study has shown that the cell volume is a strong biomarker for tumor malignancy and how a tumor will respond to treatments where larger cells were resistant to chemotherapy [12]. On the other hand, compressive stresses exerted on a cancer cell (mammary epithelial cell) by its neighboring cells and ECM have been shown to drive cancer cells toward a malignant phenotype by altering cells' motility, cell proliferation, and cell apoptosis [5], [46], [47], [48], [49], [50], [51]. Over the past two decades, the role of the mechanical phenotype of the cancer cells, their stroma, and ECM has been more appreciated [5], [43], [44], [45], [46], [47], [48]. These phenotypes are reflected in both the cell and stroma's structure and mechanics and in the biophysical properties of the cell's microenvironment, such as the mechanics and topology of the ECM. The dynamic interactions between the biophysical properties of cells, stroma, and ECM establishes a dynamic, mechanical reciprocity between the cells and their surroundings in which the cells are able to exert contractile stresses against the extracellular environment. These forces, in turn, will regulate a wide range of cellular properties that are all critical to tumorigenesis, including size, shape, volume, motility, proliferation, and differentiation [57], [58], [75], [81], [86], [87], [88], [89], [90], [91], [92], [93], [94], [95], [96], [97], [98]. Mechanical properties of tumor cells, fibroblasts, and ECM have been

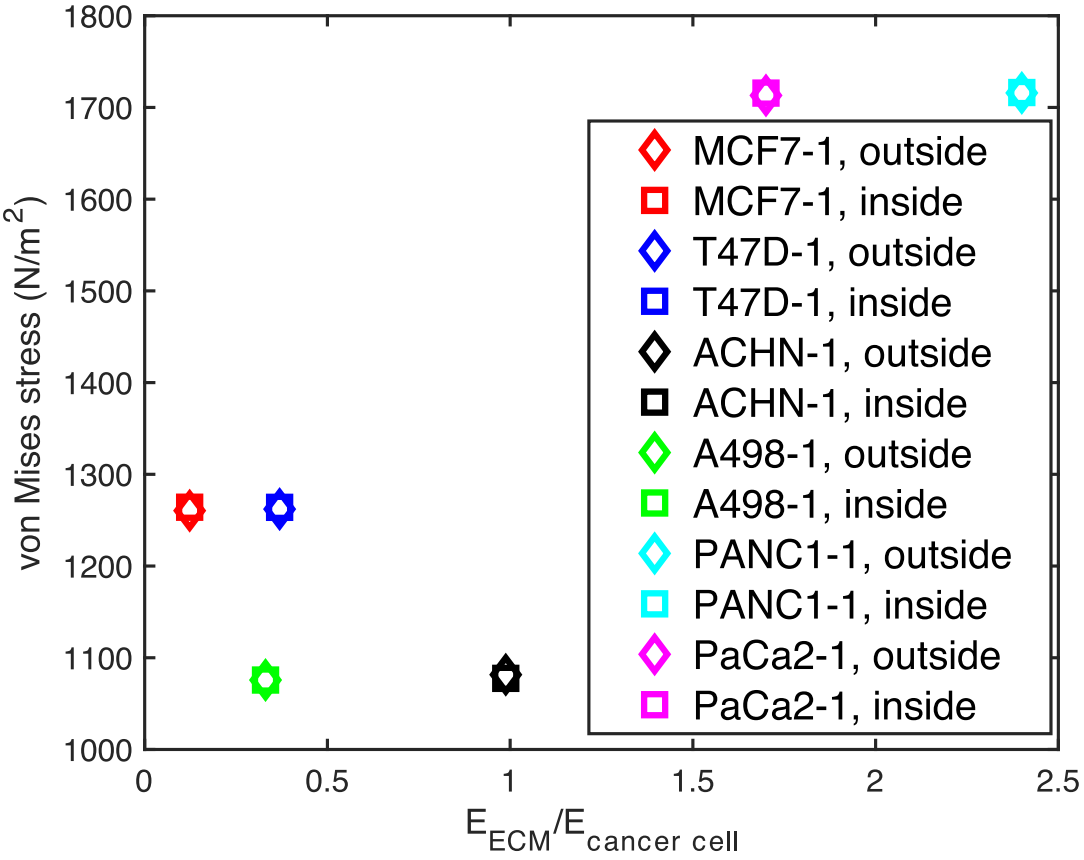

FIGURE 5. **The averaged von Mises stress values over whole tumor tissue. Note that "inside" here means the cancer cell is in contact with the surrounding fibroblasts and "outside" means that the cancer cell is in contact with the ECM.**

reported to alter the forces that each component experiences and exerts on its surroundings. However, it is still not completely understood how the organ-specific ECM may impact the forces experienced by cancer cells at different states of malignancy or if the forces experienced by the ECM are impacted by the cancer cell's malignancy state. Therefore, understanding the crosstalk between cancer cells, fibroblasts, and ECM was our main objective.

Our results (Figures 2-5) show that the ECM impacts the stresses experienced by the cancer cell, significantly. When the ECM is soft (e.g., in pancreas), the cancer cell and the fibroblasts experienced the highest stress compared to the tissues whose ECM was stiffer (e.g., in kidney). One striking point is that the stiffness of the cancer cell does not dramatically alter the forces that the cell experiences, for example, the pancreatic cancer cell line MIA-PaCa-2, with a Young's modulus of 1.7 kPa, experienced significantly higher stress values compared to the breast cancer cell line T47D with a Young's modulus of 1.2 kPa. This was also seen with the pancreatic cancer cell line PANC-1 with a Young's modulus of 1.7 kPa and kidney cancer cell line A-498 with a Young's modulus of 2.48 kPa. Furthermore, we examined the impact of the cancer cell's malignancy state in different organs and observed that a cancer cell with higher invasiveness generates higher stresses on fibroblasts and the ECM.

Our examination on the impact on cancer cell location on generated forces showed that when the cancer cell was located in contact with ECM (the outer most layer), the cancer cell and fibroblasts experienced higher stresses compared to cases where the cancer cell (central cancer cell) was only in contact with fibroblasts. The maximum stresses within pancreatic tumor tissue were observed for the pancreatic cancer cell PANC-1 as 3,750 N/m^2 and 7,500 N/m^2 for the boundary load of 10 mmHg and 20 mmHg, respectfully, which was located in contact with ECM. When the cancer cell was completely surrounded by fibroblasts, the maximum stresses within pancreatic tumor tissue was roughly 3,200 N/m^{2}and 6,500 N/m^2 for the boundary load of 10 mmHg and 20 mmHg, respectfully. It should be noted, however, that even though the cancer cell experienced slightly less stress when surrounded by fibroblasts, larger areas of stroma experienced higher stresses. As seen in Figures 2-3, the area of tumor stroma experiencing high stresses has a maximum length of 40 μm when the cancer cell is surrounded by fibroblasts and 12 μm for when the cancer cell is in vicinity of ECM.

Our further examination to find out the impact of cancer cell stiffness on stresses experienced by each organ-specific tissue is shown in Figure 5. The von Mises stresses are averaged over the whole tumor tissue. While the cancer cell's location and malignancy did not have significant impact on

IEEE Journal of Translational Engineering in Health and Medicine

the averaged magnitude of von Mises stresses over the whole tumor tissues, ECM's stiffness significantly altered these stresses. Pancreas, with a softer ECM and higher ratio of ECM stiffness to cancer cell stiffness, experienced higher stresses than both kidney and breast. Breast has softer ECM with softer cancer cells than kidney thus even though the ratio of ECM stiffness to cancer cell stiffness is lower for breast, the tumor tissue experienced generally higher stresses.

Lastly, our results showed that when adjusting the boundary load representing blood pressure within the capillaries, the stress imposed onto the tumor tissue changes. When increasing the pressure from 10 mmHg to 20 mmHg, the stress imposed on the tumor tissue almost doubled or more. Our main goal of examining impact of pressure magnitude is to mimic a tumor microenvironment for a hypertensive patient. This can enhance our knowledge on the comorbidity of hypertension and some specific types of cancer. It has been shown that patients with hypertension, have worse overall survival rates of organ-specific cancer [42], [99], [100], [101], [102]. It has also been shown that with respect to kidney cancer, hypertension, independently was associated with increased tumor size, higher tumor grade, increased nephrometry score and non-clear histology [101], [102]. Our results show that stress in both the cancer cell and their stroma increases under hypertension.

Prior studies have analyzed the effects of mechanical properties and solid stress on cancer cells and fibroblasts *in-vitro and in-vivo* [103] where cancer cells are grown in a polymer gel as spheroids. This leads to the development of solid stress that resists the spheroid expansion.Cheng et al. [104] estimated that when breast cancer cells were growing in a 0.5% agarose matrix, it was estimated that the solid stress was about 3.73 kPa when applying pressures ranging from 0 mmHg to 60 mmHg. This is in good agreement with the findings of current study. Showing that when a 20 mmHg boundary load was applied, the breast cancer cell experienced about 2,500-3,100 N/m^2(2.5-3.1 kPa) solid stress. Another study *(in vivo/in situ)* mapped the solid stress in pancreatic ductal adenocarcinoma with AK4.4 cells and found that the solid stress in the z-direction ranged from -3.60 to +7.50 kPa [105], which is in good agreement with the current study's findings as seen in Figures 2E-F and Figures 3E-F. Overall, they found that primary pancreatic tumors experienced higher solid stress compared to tumors in other metastatic sites [105]. Our results showed that pancreatic cancer cell experienced the highest solid stress levels regardless of location of cell.

There were a few limitations of the present study. First, the three-dimensional computational model did not fully represent the patient-specific complexity of the cellular microenvironment. In this model, ECM was assumed as a homogeneous media not including important microvascular structures seen within the ECM, such as fiber-forming elements (collagen and elastin) surrounded by various filling molecules (glycoproteins and proteoglycans), growth factors, and adhesion molecules. Another limitation is that the present study considered same properties for fibroblasts in all organ-specific tissues due to lack of available experimental data. Breast, kidney, and pancreas tissues are predominantly composed of fibroblasts. Other cell types exist in the tumor stroma such as endothelial cells and immune cells, but the majority of stromal cells are fibroblasts [106]. This study models the tumor microenvironment predominantly composed of fibroblasts. We assumed that the cancer cell and fibroblasts have the same shape and are modeled as hexagonal. This *in silico* model of microenvironment also did not consider vessels present in the tumor microenvironment which is because of the limitations of currently available imaging techniques for not detecting small vessels formed in the tumor microenvironment. In tumor tissues, ECM may be present between sheets of cancer cells and fibroblasts (in +/- z axis) rather than only around in x and y (as seen in Figure 1). These structures are seen in tumors with loose stroma when fibroblasts do not form a complete fibrous layer. In this study, we considered that the tumor stroma is consisting of a thick fibrous layer and that a cancer cell is either entirely surrounded by fibroblasts or exposed to ECM on one side. Our model is attempting to quantify the forces that a cancer cell and their stroma experiences at distinct stages of malignancy. This model is not monitoring cancer cell growth. In this study, we used different cell lines representing distinct stages of tumor malignancy and for different organs. We did not consider cancer cells' genetic changes and we did not examine the cancer cell's response to any drug. Nonetheless, we have been able to gain important insights into dynamic interactions between a cancer cell and its microenvironment. The clinical significance of including different cell lines for our model is that differences in properties of cancer cells and ECM impact cell-cell and cell-ECM interactions. These properties may well represent the discrepancies observed across large patient populations.

IV. CONCLUSION

In conclusion, our results show that heterogeneity of the cancer cell, fibroblasts, and ECM properties, representing different organ-specific biological conditions and malignancy states, impact the stresses that these tumor tissue components exert on each other. Our study reveals that the stresses experienced by the cancer cell and fibroblasts can be controlled by altering their microenvironment. We have revealed that the ECM stiffness influences stresses exerted on fibroblasts and the cancer cells while the malignant cancer cell generates higher stresses on its stroma. To our knowledge, this is the first study that quantifies stresses experienced by individual tumor components, and it will serve as an important first step in understanding of how the stresses experienced by the cancer cell and stroma are associated with malignancy states of cancer cells in different organs. The three-dimensional, multicomponent, computational model used in the present study has the potential to further study highly complex tumor microenvironments in cancers that are severely understudied,

such as pancreatic ductal adenocarcinoma, and will bring light to the critical role of physical stresses on tumor growth and their importance as potential biomarkers to determine tumor malignancy. Our study takes the first important step in understanding what factors could be impacting cancer treatments or even biomarkers to be looking for. Furthermore, our *in silico* model of tumor microenvironment can yield critical, useful information for guiding *ex vivo* or *in vitro* experiments and narrow down variables to be investigated.

CONFLICT OF INTEREST

The authors declares that they have no financial, professional, or personal conflict of interest.

AUTHOR CONTRIBUTIONS

Conception and design: Mahsa Dabagh; Acquisition of data: Morgan Connaughton; Analysis and interpretation of data: Morgan Connaughton and Mahsa Dabagh; Literature Search: Morgan Connaughton and Mahsa Dabagh; Drafting the article: Morgan Connaughton and Mahsa Dabagh; Critically revising the article: Mahsa Dabagh; Reviewed submitted version of manuscript: Mahsa Dabagh; Approved the final version of the manuscript on behalf of all authors: Mahsa Dabagh; Study supervision: Mahsa Dabagh; Funds Collection: Mahsa Dabagh.

CITATION DIVERSITY STATEMENT

Recent work in several fields of science has identified a bias in citation practices such that papers from women and other minority scholars are undercited relative to the number of papers in the field. The authors recognize this bias and have worked diligently to ensure that they are referencing appropriate papers with fair gender and racial author inclusion.

HUMAN STUDIES

No human studies were carried out by the authors for this article.

ANIMAL STUDIES

No animal studies were carried out by the authors for this article.

ETHICAL STATEMENT

None

REFERENCES

[1] *World Health Organization*. Accessed: Sep. 2023. [Online]. Available: https://www.who.int/news-room/fact-sheets/detail/cancer

[2] A. McGuigan, P. Kelly, R. C. Turkington, C. Jones, H. G. Coleman, and R. S. McCain, "Pancreatic cancer: A review of clinical diagnosis, epidemiology, treatment and outcomes," *World J. Gastroenterol.*, vol. 24, no. 43, pp. 4846–4861, Nov. 2018, doi: 10.3748/wjg.v24.i43.4846.

[3] S. Wang et al., "The molecular biology of pancreatic adenocarcinoma: Translational challenges and clinical perspectives," *Signal Transduction Targeted Therapy*, vol. 6, no. 1, p. 249, Jul. 2021, doi: 10.1038/s41392-021-00659-4.

[4] Y. Lyu, Q. Xiao, Y. Li, Y. Wu, W. He, and L. Yin, "'Locked' cancer cells are more sensitive to chemotherapy," *Bioeng. Transl. Med.*, vol. 4, no. 2, 2019, Art. no. e10130, doi: 10.1002/btm2.10130.

[5] S. Kumar and V. M. Weaver, "Mechanics, malignancy, and metastasis: The force journey of a tumor cell," *Cancer Metastasis Rev.*, vol. 28, pp. 113–127, Jun. 2009, doi: 10.1007/s10555-008-9173-4.

[6] J. R. Lange and B. Fabry, "Cell and tissue mechanics in cell migration," *Experim. Cell Res.*, vol. 319, no. 16, pp. 2418–2423, Oct. 2013, doi: 10.1016/j.yexcr.2013.04.023.

[7] S. F. Pedersen, E. K. Hoffmann, and I. Novak, "Cell volume regulation in epithelial physiology and cancer," *Frontiers Physiol.*, vol. 4, p. 56885, Aug. 2013, doi: 10.3389/fphys.2013.00233.

[8] J. Makki, "Diversity of breast carcinoma: Histological subtypes and clinical relevance," *Clin. Med. Insights, Pathol.*, vol. 8, Jan. 2015, Art. no. CPath.S31563, doi: 10.4137/cpath.s31563.

[9] J. Adjo Aka and S.-X. Lin, "Comparison of functional proteomic analyses of human breast cancer cell lines T47D and MCF7," *PLoS ONE*, vol. 7, no. 2, Feb. 2012, Art. no. e31532, doi: 10.1371/journal.pone.0031532.

[10] S. Nallanthighal, J. P. Heiserman, and D.-J. Cheon, "The role of the extracellular matrix in cancer stemness," *Frontiers Cell Develop. Biol.*, vol. 7, p. 86, Jul. 2019, doi: 10.3389/fcell.2019.00086.

[11] K. Morishita, K. Watanabe, and H. Ichijo, "Cell volume regulation in cancer cell migration driven by osmotic water flow," *Cancer Sci.*, vol. 110, no. 8, pp. 2337–2347, Aug. 2019, doi: 10.1111/cas.14079.

[12] *Cancer Cells Shrink or Super-Size to Survive*. Accessed: Apr. 2023. [Online]. Available: https://www.icr.ac.uk/news-archive/cancer-cells-shrink-or-super-size-to-survive

[13] D. Delle Cave, R. Rizzo, B. Sainz, G. Gigli, L. L. del Mercato, and E. Lonardo, "The revolutionary roads to study cell–cell interactions in 3D in vitro pancreatic cancer models," *Cancers*, vol. 13, no. 4, p. 930, Feb. 2021, doi: 10.3390/cancers13040930.

[14] K. P. Pednekar, M. A. Heinrich, J. van Baarlen, and J. Prakash, "Novel 3D μtissues mimicking the fibrotic stroma in pancreatic cancer to study cellular interactions and stroma-modulating therapeutics," *Cancers*, vol. 13, no. 19, p. 5006, Oct. 2021, doi: 10.3390/cancers13195006.

[15] B. Gundel, X. Liu, M. Lohr, and R. Heuchel, "Pancreatic ductal adenocarcinoma: Preclinical in vitro and ex vivo models," *Front. Cell Dev. Biol.*, vol. 9, Oct. 2021, Art. no. 741162, doi: 10.3389/fcell.2021.741162.

[16] M. A. Heinrich, A. M. R. H. Mostafa, J. P. Morton, L. J. A. C. Hawinkels, and J. Prakash, "Translating complexity and heterogeneity of pancreatic tumor: 3D in vitro to in vivo models," *Adv. Drug Del. Rev.*, vol. 174, pp. 265–293, Jul. 2021, doi: 10.1016/j.addr.2021.04.018.

[17] E. M. Langer et al., "Modeling tumor phenotypes in vitro with three-dimensional bioprinting," *Cell Rep.*, vol. 26, no. 3, pp. 608–623, Jan. 2019, doi: 10.1016/j.celrep.2018.12.090.

[18] D. O. de la Pena et al., "Bioengineered 3D models of human pancreatic cancer recapitulate in vivo tumour biology," *Nature Commun.*, vol. 12, no. 1, p. 5623, 2021, doi: 10.1038/s41467-021-25921-9.

[19] J. Kokkinos et al., "Ex vivo culture of intact human patient derived pancreatic tumour tissue," *Sci. Rep.*, vol. 11, p. 1944, Jan. 2021, doi: 10.1038/s41598-021-81299-0.

[20] A. Shirinifard, J. S. Gens, B. L. Zaitlen, N. J. Poplawski, M. Swat, and J. A. Glazier, "3D multi-cell simulation of tumor growth and angiogenesis," *PLoS ONE*, vol. 4, no. 10, p. e7190, Oct. 2009, doi: 10.1371/journal.pone.0007190.

[21] M. Fritz, P. K. Jha, T. Köppl, J. T. Oden, and B. Wohlmuth, "Analysis of a new multispecies tumor growth model coupling 3D phase-fields with a 1D vascular network," *Nonlinear Anal., Real World Appl.*, vol. 61, Oct. 2021, Art. no. 103331, doi: 10.1016/j.nonrwa.2021.103331.

[22] F. Iranmanesh and M. A. Nazari, "Finite element modeling of avascular tumor growth using a stress-driven model," *J. Biomechanical Eng.*, vol. 139, no. 8, Aug. 2017, Art. no. 081009, doi: 10.1115/1.4037038.

[23] I. Hidrovo et al., "Experimental method and statistical analysis to fit tumor growth model using SPECT/CT imaging: A preclinical study," *Quant. Imag. Med. Surg.*, vol. 7, p. 299, Jun. 2017, doi: 10.21037/qims.2017.06.05.

[24] H. Murphy, H. Jaafari, and H. M. Dobrovolny, "Differences in predictions of ODE models of tumor growth: A cautionary example," *BMC Cancer*, vol. 16, no. 1, p. 163, Dec. 2016, doi: 10.1186/s12885-016-2164-x.

[25] Y. Watanabe, E. L. Dahlman, K. Z. Leder, and S. K. Hui, "A mathematical model of tumor growth and its response to single irradiation," *Theor. Biol. Med. Model.*, vol. 13, pp. 1–20, Dec. 2016, doi: 10.1186/s12976-016-0032-7.

[26] A. V. P. Bobadilla, R. Doursat, and F. Amblard, "An agent-based model of avascular tumor growth," in *Proc. Eur. Conf. Artif. Life*, Jul. 2015, pp. 648–655, doi: 10.7551/978-0-262-33027-5-ch114.

IEEE Journal of Translational Engineering in Health and Medicine

[27] Y. Jiang, J. Pjesivac-Grbovic, C. Cantrell, and J. P. Freyer, "A multiscale model for avascular tumor growth," *Biophysical J.*, vol. 89, no. 6, pp. 3884–3894, Dec. 2005, doi: 10.1529/biophysj.105.060640.

[28] S. Patmanidis, A. C. Charalampidis, I. Kordonis, G. D. Mitsis, and G. P. Papavassilopoulos, "Tumor growth modeling: Parameter estimation with maximum likelihood methods," *Comput. Methods Programs Biomed.*, vol. 160, pp. 1–10, Jul. 2018, doi: 10.1016/j.cmpb.2018.03.014.

[29] B. Medha, D. Chandana, V. Sowmya, W. W. Godfrey, G. Kaushal, and J. Dhar, "Tumor growth modeling and estimation of changes with respect to cytotoxic drugs," in *Proc. IEEE Region 10 Conf. (TENCON)*, Oct. 2019, pp. 1053–1058, doi: 10.1109/TENCON.2019.8929486.

[30] J. Metzcar, Y. Wang, R. Heiland, and P. Macklin, "A review of cell-based computational modeling in cancer biology," *JCO Clin. Cancer Inform.*, vol. 3, pp. 1–13, Feb. 2019, doi: 10.1200/CCI.18.00069.

[31] S. J. Nivlouei, M. Soltani, J. Carvalho, R. Travasso, M. R. Salimpour, and E. Shirani, "Multiscale modeling of tumor growth and angiogenesis: Evaluation of tumor-targeted therapy," *PLoS Comput. Biol.*, vol. 17, no. 6, 2021, Art. no. e1009081, doi: 10.1371/journal.pcbi.1009081.

[32] S. Bekisz and L. Geris, "Cancer modeling: From mechanistic to data-driven approaches, and from fundamental insights to clinical applications," *J. Comput. Sci.*, vol. 46, Oct. 2020, Art. no. 101198.

[33] J. Tan, T. R. Sinno, and S. L. Diamond, "A parallel fluid-solid coupling model using LAMMPS and Palabos based on the immersed boundary method," *J. Comput. Sci.*, vol. 25, pp. 89–100, Mar. 2018.

[34] B. Gompertz, "XXIV. On the nature of the function expressive of the law of human mortality, and on a new mode of determining the value of life contingencies," *Philos. Trans. Roy. Soc. London*, vol. 115, pp. 513–583, Dec. 1825, doi: 10.1098/rstl.1825.0026.

[35] S. C. Ferreira Jr., M. L. Martins, and M. J. Vilela, "Reaction-diffusion model for the growth of avascular tumor," *Phys. Rev. E, Stat. Phys. Plasmas Fluids Relat. Interdiscip. Top.*, vol. 65, no. 2, 2002, Art. no. 021907, doi: 10.1103/PhysRevE.65.021907.

[36] F. J. Vermolen, R. P. Meijden, M. Es, A. Gefen, and D. Weihs, "Towards a mathematical formalism for semi-stochastic cell-level computational modeling of tumor initiation," *Ann. Biomed. Eng.*, 43, pp. 1680–1694, Jul. 2015, doi: 10.1007/s10439-015-1271-1.

[37] C. A. Athale and T. S. Deisboeck, "The effects of EGF-receptor density on multiscale tumor growth patterns," *J. Theor. Biol.*, vol. 238, no. 4, pp. 771–779, Feb. 2006, doi: 10.1016/j.jtbi.2005.06.029.

[38] A. Szabó and R. M. H. Merks, "Cellular Potts modeling of tumor growth, tumor invasion, and tumor evolution," *Frontiers Oncol.*, vol. 3, p. 87, Apr. 2013, doi: 10.3389/fonc.2013.00087.

[39] C. T. Mierke, "Viscoelasticity, like forces, plays a role in mechanotransduction," *Frontiers Cell Developmental Biol.*, vol. 10, Feb. 2022, Art. no. 789841, doi: 10.3389/fcell.2022.789841.

[40] P. Manoukian, M. Bijlsma, and H. Van Laarhoven, "The cellular origins of cancer-associated fibroblasts and their opposing contributions to pancreatic cancer growth," *Frontiers Cell Developmental Biol.*, vol. 9, Feb. 2021, Art. no. 743907, doi: 10.3389/fcell.2021.743907.

[41] B. Jiang et al., "Stroma-targeting therapy in pancreatic cancer: One coin with two sides?" *Frontiers Oncol.*, vol. 10, Oct. 2020, Art. no. 576399, doi: 10.3389/fonc.2020.576399.

[42] X. Hu et al., "Tailor-made nanomaterials for diagnosis and therapy of pancreatic ductal adenocarcinoma," *Adv. Sci.*, vol. 8, Apr. 2021, Art. no. 2002545, doi: 10.1002/advs.202002545.

[43] H. Y. Tanaka and M. R. Kano, "Stromal barriers to nanomedicine penetration in the pancreatic tumor microenvironment," *Cancer Sci.*, vol. 109, pp. 2085–2092, Jul. 2018, doi: 10.1111/cas.13630.

[44] L. M. Rebelo, J. S. de Sousa, J. M. Filho, and M. Radmacher, "Comparison of the viscoelastic properties of cells from different kidney cancer phenotypes measured with atomic force microscopy," *Nanotechnology*, vol. 24, no. 5, Feb. 2013, Art. no. 055102, doi: 10.1088/0957-4484/24/5/055102.

[45] R. K. Jain, J. D. Martin, and T. Stylianopoulos, "The role of mechanical forces in tumor growth and therapy," *Annu. Rev. Biomed. Eng.*, vol. 16, pp. 46–321, Jul. 2014, doi: 10.1146/annurev-bioeng-071813-105259.

[46] J. M. Tse et al., "Mechanical compression drives cancer cells toward invasive phenotype," *Proc. Nat. Acad. Sci. USA*, vol. 109, no. 3, pp. 911–916, Jan. 2012, doi: 10.1073/pnas.1118910109.

[47] V. F. Fiore et al., "Mechanics of a multilayer epithelium instruct tumour architecture and function," *Nature*, vol. 585, pp. 433–439, Sep. 2020, doi: 10.1038/s41586-020-2695-9.

[48] E. Jonietz, "Mechanics: The forces of cancer," *Nature*, vol. 491, pp. 56–57, Nov. 2012, doi: 10.1038/491S56a.

[49] R. Sinha et al., "Analysis of renal cancer cell lines from two major resources enables genomics-guided cell line selection," *Nat Commun.*, vol. 8, no. 1, pp. 1–10, 2017, doi: 10.1038/ncomms15165.

[50] M. Chuang et al., "Tumor-derived tumor necrosis factor-alpha promotes progression and epithelial-mesenchymal transition in renal cell carcinoma cells," *Cancer Sci.*, vol. 99, no. 5, pp. 905–913, May 2008, doi: 10.1111/j.1349-7006.2008.00756.x.

[51] M. C. Cho et al., "EphA2 is a potential player of malignant cellular behavior in non-metastatic renal cell carcinoma cells but not in metastatic renal cell carcinoma cells," *PLoS ONE*, vol. 10, no. 7, Jul. 2015, Art. no. e0130975, doi: 10.1371/journal.pone.0130975.

[52] L. A. Gordon, K. T. Mulligan, H. Maxwell-Jones, M. Adams, R. A. Walker, and J. L. Jones, "Breast cell invasive potential relates to the myoepithelial phenotype," *Int. J. Cancer*, vol. 106, no. 1, pp. 8–16, Aug. 2003, doi: 10.1002/ijc.11172.

[53] D. Kpeglo et al., "Modeling the mechanical stiffness of pancreatic ductal adenocarcinoma," *Matrix Biol. Plus*, vol. 14, Jun. 2022, Art. no. 100109, doi: 10.1016/j.mbplus.2022.100109.

[54] R. Gradiz, H. C. Silva, L. Carvalho, M. F. Botelho, and A. Mota-Pinto, "MIA PaCa-2 and PANC-1—Pancreas ductal adenocarcinoma cell lines with neuroendocrine differentiation and somatostatin receptors," *Sci. Rep.*, vol. 6, no. 1, p. 21648, Feb. 2016, doi: 10.1038/srep21648.

[55] A. V. Nguyen et al., "Stiffness of pancreatic cancer cells is associated with increased invasive potential," *Integrative Biol.*, vol. 8, no. 12, pp. 1232–1245, 2016, doi: 10.1039/c6ib00135a.

[56] B. I. Shraiman, "Mechanical feedback as a possible regulator of tissue growth," *Proc. Nat. Acad. Sci. USA*, vol. 102, no. 9, pp. 3318–3323, 2005.

[57] R. Levayer, "Solid stress, competition for space and cancer: The opposing roles of mechanical cell competition in tumour initiation and growth," *Seminars Cancer Biol.*, vol. 63, pp. 69–80, Jun. 2020, doi: 10.1016/j.semcancer.2019.05.004.

[58] K. Bacevic et al., "Spatial competition constrains resistance to targeted cancer therapy," *Nat. Commun.*, vol. 8, p. 1995, Dec. 2017.

[59] A. Alonso, A. Ebben, and M. Dabagh, "Impact of disturbed flow and arterial stiffening on mechanotransduction in endothelial cells," *Biomechanics Model. Mechanobiol.*, vol. 22, no. 6, pp. 1919–1933, 2023, doi: 10.1007/s10237-023-01743-0.

[60] A. Ebben and M. Dabagh, "Mechanotransduction in endothelial cells in vicinity of cancer cells," *Cellular Mol. Bioeng.*, vol. 15, pp. 313–330, Aug. 2022, doi: 10.1007/s12195-022-00728-w.

[61] M. Dabagh, P. Jalali, P. J. Butler, A. Randles, and J. M. Tarbell, "Mechanotransmission in endothelial cells subjected to oscillatory and multi-directional shear flow," *J. Roy. Soc. Interface*, vol. 14, no. 130, 2017, Art. no. 20170185.

[62] M. Dabagh, P. Jalali, P. J. Butler, and J. M. Tarbell, "Shear-induced force transmission in a multicomponent, multicell model of the endothelium," *J. Roy. Soc. Interface*, vol. 11, no. 98, 2014, Art. no. 20140431.

[63] M. Dabagh, J. Gounley, and A. Randles, "Localization of rolling and firm-adhesive interactions between circulating tumor cells and the microvasculature wall," *Cellular Mol. Bioeng.*, vol. 13, pp. 141–154, Apr. 2020.

[64] P. Guo, B. Cai, M. Lei, Y. Liu, and B. M. Fu, "Differential arrest and adhesion of tumor cells and microbeads in the microvasculature," *Biomech. Model. Mechanobiol.*, vol. 13, no. 3, pp. 537–550, 2014.

[65] N. Takeishi, Y. Imai, S. Ishida, T. Omori, R. D. Kamm, and T. Ishikawa, "Cell adhesion during bullet motion in capillaries," *Amer. J. Physiology-Heart Circulatory Physiol.*, vol. 311, no. 2, pp. 395–403, Aug. 2016.

[66] W. W. Yan, B. Cai, Y. Liu, and B. M. Fu, "Effects of wall shear stress and its gradient on tumor cell adhesion in curved microvessels," *Biomechanics Model. Mechanobiol.*, vol. 11, no. 5, pp. 641–653, May 2012.

[67] F. L. H. Brown, "Elastic modeling of biomembranes and lipid bilayers," *Annu. Rev. Phys. Chem.*, vol. 59, pp. 685–712, May 2008, doi: 10.1146/annurev.physchem.59.032607.093550.

[68] T. G. Kuznetsova, M. N. Starodubtseva, N. I. Yegorenkov, S. A. Chizhik, and R. I. Zhdanov, "Atomic force microscopy probing of cell elasticity," *Micron*, vol. 38, no. 8, pp. 824–833, Dec. 2007, doi: 10.1016/j.micron.2007.06.011.

[69] K. Pogoda et al., "Depth-sensing analysis of cytoskeleton organization based on AFM data," *Eur. Biophys. J.*, vol. 41, no. 1, pp. 79–87, Jan. 2012, doi: 10.1007/s00249-011-0761-9.

[70] F.-S. Quan and K. S. Kim, "Medical applications of the intrinsic mechanical properties of single cells," *Acta Biochimica et Biophysica Sinica*, vol. 48, no. 10, pp. 865–871, Oct. 2016, doi: 10.1093/abbs/gmw081.

[71] S. Kwon, W. Yang, D. Moon, and K. S. Kim, "Comparison of cancer cell elasticity by cell type," *J. Cancer*, vol. 11, no. 18, pp. 5403–5412, 2020, doi: 10.7150/jca.45897.

[72] D. T. Dibaba, K. Ogunsina, D. Braithwaite, and T. Akinyemiju, "Metabolic syndrome and risk of breast cancer mortality by menopause, obesity, and subtype," *Breast Cancer Res. Treatment*, vol. 174, no. 1, pp. 209–218, Feb. 2019, doi: 10.1007/s10549-018-5056-8.

[73] A. Samani, J. Zubovits, and D. Plewes, "Elastic moduli of normal and pathological human breast tissues: An inversion-technique-based investigation of 169 samples," *Phys. Med. Biol.*, vol. 52, no. 6, pp. 1565–1576, Mar. 2007, doi: 10.1088/0031-9155/52/6/002.

[74] P. N. T. Wells and H.-D. Liang, "Medical ultrasound: Imaging of soft tissue strain and elasticity," *J. Roy. Soc. Interface*, vol. 8, no. 64, pp. 1521–1549, Nov. 2011, doi: 10.1098/rsif.2011.0054.

[75] A. M. Handorf, Y. Zhou, M. A. Halanski, and W.-J. Li, "Tissue stiffness dictates development, homeostasis, and disease progression," *Organogenesis*, vol. 11, no. 1, pp. 1–15, Jan. 2015, doi: 10.1080/15476278.2015.1019687.

[76] A. J. Rice et al., "Matrix stiffness induces epithelial–mesenchymal transition and promotes chemoresistance in pancreatic cancer cells," *Oncogenesis*, vol. 6, no. 7, pp. 352, Jul. 2017, doi: 10.1038/oncsis.2017.54.

[77] A. Gefen and B. Dilmoney, "Mechanics of the normal woman's breast," *Technol. Health Care*, vol. 15, no. 4, pp. 259–271, Jul. 2007, doi: 10.3233/thc-2007-15404.

[78] N. W. Tschoegl, W. G. Knauss, and I. Emri, "Poisson's ratio in linear viscoelasticity—A critical review," *Time-Dependent Mater.*, vol. 6, pp. 3–51, Mar. 2002, doi: 10.1023/A:1014411503170.

[79] R. A. E. Edden, S. A. Smith, and P. B. Barker, "Longitudinal and multi-echo transverse relaxation times of normal breast tissue at 3 Tesla," *J. Magn. Reson. Imag.*, vol. 32, no. 4, pp. 982–987, Oct. 2010, doi: 10.1002/jmri.22306.

[80] J. Z. Bojorquez, S. Bricq, C. Acquitter, F. Brunotte, P. M. Walker, and A. Lalande, "What are normal relaxation times of tissues at 3 T?" *Magn. Reson. Imag.*, vol. 35, pp. 69–80, Jan. 2017, doi: 10.1016/j.mri.2016.08.021.

[81] G.-F. Xiong and R. Xu, "Function of cancer cell-derived extracellular matrix in tumor progression," *J. Cancer Metastasis Treatment*, vol. 2, no. 9, p. 357, Sep. 2016, doi: 10.20517/2394-4722.2016.08.

[82] A. C. Shore, "Capillaroscopy and the measurement of capillary pressure," *Brit. J. Clin. Pharmacol.*, vol. 50, no. 6, pp. 501–513, Dec. 2000, doi: 10.1046/j.1365-2125.2000.00278.x.

[83] M. Dabagh, J. Gounley, and A. Randles, "Multiscale modeling of interactions between deformable cancer cell and the vessel wall," in *Proc. BMES Annu. Meeting*, Phoenix, AZ USA, Oct. 2014, pp. 1–10.

[84] D. Puleri, M. Dabagh, and A. Randles, "Computational methods to model cell adhesion with varying receptor patterns," in *Proc. BMES*, Oct. 2018, pp. 1–8.

[85] M. Dabagh and A. Randles, "Role of deformable cancer cells on wall shear stress-associated-VEGF secretion by endothelium in microvasculature," *PLOS ONE*, vol. 14, Feb. 2019, Art. no. e0211418.

[86] J. Winkler, A. Abisoye-Ogunniyan, K. J. Metcalf, and Z. Werb, "Concepts of extracellular matrix remodelling in tumour progression and metastasis," *Nature Commun.*, vol. 11, no. 1, p. 5120, Oct. 2020, doi: 10.1038/s41467-020-18794-x.

[87] W. Xu, R. Mezencev, B. Kim, L. Wang, J. McDonald, and T. Sulchek, "Cell stiffness is a biomarker of the metastatic potential of ovarian cancer cells," *PLoS ONE*, vol. 7, no. 10, Oct. 2012, Art. no. e46609, doi: 10.1371/journal.pone.0046609.

[88] L. Wullkopf et al., "Cancer cells' ability to mechanically adjust to extracellular matrix stiffness correlates with their invasive potential," *Mol. Biol. Cell*, vol. 29, no. 20, pp. 2378–2385, Oct. 2018, doi: 10.1091/mbc.e18-05-0319.

[89] N. M. Anderson and M. C. Simon, "The tumor microenvironment," *Current Biol.*, vol. 30, no. 16, pp. 921–925, Aug. 2020, doi: 10.1016/j.cub.2020.06.081.

[90] J. Huang et al., "Extracellular matrix and its therapeutic potential for cancer treatment," *Signal Transduction Targeted Therapy*, vol. 6, no. 1, p. 153, Apr. 2021, doi: 10.1038/s41392-021-00544-0.

[91] M. W. Conklin et al., "Aligned collagen is a prognostic signature for survival in human breast carcinoma," *Amer. J. Pathol.*, vol. 178, no. 3, pp. 1221–1232, Mar. 2011, doi: 10.1016/j.ajpath.2010.11.076.

[92] T. Su, B. Yang, T. Gao, T. Liu, and J. Li, "Polymer nanoparticle-assisted chemotherapy of pancreatic cancer," *Therapeutic Adv. Med. Oncol.*, vol. 12, pp. 1–33, May 2020, doi: 10.1177/1758835920915978.

[93] S. Bhattacharyya et al., "Acidic fibroblast growth factor underlies microenvironmental regulation of MYC in pancreatic cancer," *J. Exp. Med.*, vol. 217, Aug. 2020, Art. no. e20191805, doi: 10.1084/jem.20191805.

[94] S. Kunjachan et al., "Selective priming of tumor blood vessels by radiation therapy enhances nanodrug delivery," *Sci. Rep.*, vol. 9, p. 15844, Sep. 2019, doi: 10.1038/s41598-019-50538-w.

[95] R. Sobreiro-Almeida, R. Quinteira, and N. M. Neves, "Renal regeneration: The role of extracellular matrix and current ECM-based tissue engineered strategies," *Adv. Healthcare Mater.*, vol. 10, no. 14, 2021, Art. no. 2100160, doi: 10.1002/adhm.202100160.

[96] P. Taufalele et al., "Matrix stiffness enhances cancer-macrophage interactions and M2-like macrophage accumulation in the breast tumor microenvironment," *Acta Biomaterialia*, vol. 163, pp. 365–377, Jun. 2022, doi: 10.1016/j.actbio.2022.04.031.

[97] J. M. Hope et al., "Fluid shear stress enhances T cell activation through Piezo1," *BMC Biol.*, vol. 20, p. 61, Mar. 2022, doi: 10.1186/s12915-022-01266-7.

[98] J. D. Greenlee, K. Liu, M. Lopez-Cavestany, and M. R. King, "Piezo1 mechano-activation is augmented by resveratrol and differs between colorectal cancer cells of primary and metastatic origin," *Molecules*, vol. 27, p. 5430, Aug. 2022, doi: 10.3390/molecules27175430.

[99] T. Stocks et al., "Blood pressure and risk of cancer incidence and mortality in the metabolic syndrome and cancer project," *Hypertension*, vol. 59, no. 4, pp. 802–810, Apr. 2012, doi: 10.1161/hypertensionaha.111.189258.

[100] P. Yang et al., "A large-scale retrospective study of the overall survival outcome in nasopharyngeal carcinoma with hypertension in Chinese population," *Oncotarget*, vol. 8, no. 43, pp. 75577–75586, Sep. 2017, doi: 10.18632/oncotarget.17483.

[101] N. J. Kocher, C. Rjepaj, H. Robyak, E. Lehman, and J. D. Raman, "Hypertension is the primary component of metabolic syndrome associated with pathologic features of kidney cancer," *World J. Urol.*, vol. 35, no. 1, pp. 67–72, Jan. 2017, doi: 10.1007/s00345-016-1850-2.

[102] M. Connaughton and M. Dabagh, "Association of hypertension and organ-specific cancer: A meta-analysis," *HealthCare*, vol. 10, p. 1074, Jun. 2022, doi: 10.3390/healthcare10061074.

[103] M. Kalli and T. Stylianopoulos, "Defining the role of solid stress and matrix stiffness in cancer cell proliferation and metastasis," *Front Oncol.*, vol. 8, p. 55, Mar. 2018, doi: 10.3389/fonc.2018.00055.

[104] G. Cheng, J. Tse, R. K. Jain, and L. L. Munn, "Micro-environmental mechanical stress controls tumor spheroid size and morphology by suppressing proliferation and inducing apoptosis in cancer cells," *PLoS ONE*, vol. 4, no. 2, p. e4632, Feb. 2009, doi: 10.1371/journal.pone.0004632.

[105] H. T. Nia et al., "Solid stress and elastic energy as measures of tumour mechanopathology," *Nature Biomed. Eng.*, vol. 1, no. 1, p. 0004, Nov. 2016.

[106] Y. Mao, E. T. Keller, D. H. Garfield, K. Shen, and J. Wang, "Stromal cells in tumor microenvironment and breast cancer," *Cancer Metastasis Rev.*, vol. 32, pp. 15–303, Jun. 2013, doi: 10.1007/s10555-012-9415-3.